JEM Journal of Experimental Medicine

ARTICLE

Helicobacter pylori metabolites exacerbate gastritis through C-type lectin receptors

Masahiro Nagata[1], Kenji Toyonaga[1], Eri Ishikawa[1,2], Shojiro Haji[1,3], Nobuyuki Okahashi[4,5], Masatomo Takahashi[6], Yoshihiro Izumi[6], Akihiro Imamura[7], Koichi Takato[7], Hideharu Ishida[7,8], Shigenori Nagai[9], Petr Illarionov[10], Bridget L. Stocker[11,12,13], Mattie S.M. Timmer[11,12,13], Dylan G.M. Smith[14], Spencer J. Williams[14], Takeshi Bamba[6], Tomofumi Miyamoto[15], Makoto Arita[5,16,17], Ben J. Appelmelk[18], and Sho Yamasaki[1,2,19,20]

Helicobacter pylori **causes gastritis, which has been attributed to the development of *H. pylori*–specific T cells during infection. However, the mechanism underlying innate immune detection leading to the priming of T cells is not fully understood, as *H. pylori* evades TLR detection. Here, we report that *H. pylori* metabolites modified from host cholesterol exacerbate gastritis through the interaction with C-type lectin receptors. Cholesteryl acyl α-glucoside (αCAG) and cholesteryl phosphatidyl α-glucoside (αCPG) were identified as noncanonical ligands for Mincle (*Clec4e*) and DCAR (*Clec4b1*). During chronic infection, *H. pylori*–specific T cell responses and gastritis were ameliorated in Mincle-deficient mice, although bacterial burdens remained unchanged. Furthermore, a mutant *H. pylori* strain lacking αCAG and αCPG exhibited an impaired ability to cause gastritis. Thus *H. pylori*–specific modification of host cholesterol plays a pathophysiological role that exacerbates gastric inflammation by triggering C-type lectin receptors.**

Introduction

Helicobacter pylori is a Gram-negative pathogenic bacterium that successfully colonizes the gastric mucosa of half of the world's population. Persistent *H. pylori* infection induces chronic gastritis, which is one of most common risk factors for gastric malignancy (NIH Consensus Conference, 1994; Peek and Blaser, 2002). In addition to the virulence proteins secreted from *H. pylori* (Hatakeyama, 2004), recent studies have underscored the critical role of *H. pylori*–primed host $CD4^+$ T cells in the development of gastritis (Eaton et al., 2001; Nagai et al., 2007). However, such T cells do not efficiently contribute to the eradication of this pathogen (Adamsson et al., 2017) and are considered deleterious for the host (D'Elios et al., 2005). Hence, insight into mechanisms by which *H. pylori* primes T cells may help in the prevention of chronic gastritis and malignancy.

H. pylori avoids detection by the canonical pattern recognition receptors, TLRs, by modifying its TLR ligands (Roy and Mocarski, 2007). Instead of having typical pathogen-associated molecular patterns, *H. pylori* produces a wealth of diverse lipids, in particular assorted cholesterol metabolites (Jan et al., 2016). For example, *H. pylori* extracts cholesterol from the host and converts it to unique cholesteryl glucosides, such as cholesteryl acyl α-glucosides (αCAGs; Grille et al., 2010; Haque et al., 1996; Hirai et al., 1995; Lebrun et al., 2006; Mayberry and Smith, 1983), which are reported to suppress host immunity (Wunder

[1]Department of Molecular Immunology, Research Institute for Microbial Diseases, Osaka University, Suita, Osaka, Japan; [2]Laboratory of Molecular Immunology, Immunology Frontier Research Center, Osaka University, Suita, Osaka, Japan; [3]Department of Medicine and Bioregulatory Science, Graduate School of Medical Sciences, Kyushu University, Fukuoka, Fukuoka, Japan; [4]Department of Bioinformatics Engineering, Graduate School of Information Science and Technology, Osaka University, Suita, Osaka, Japan; [5]Laboratory for Metabolomics, RIKEN Center for Integrative Medical Sciences, Yokohama, Kanagawa, Japan; [6]Division of Metabolomics, Medical Institute of Bioregulation, Kyushu University, Fukuoka, Fukuoka, Japan; [7]Department of Applied Bioorganic Chemistry, Gifu University, Gifu, Gifu, Japan; [8]Center for Highly Advanced Integration of Nano and Life Sciences (G-CHAIN), Gifu University, Gifu, Gifu, Japan; [9]Department of Molecular Immunology, Graduate School of Medical and Dental Sciences, Tokyo Medical and Dental University, Bunkyo-ku, Tokyo, Japan; [10]School of Biosciences, University of Birmingham, Birmingham, UK; [11]School of Chemical and Physical Sciences, Victoria University of Wellington, Wellington, New Zealand; [12]Centre for Biodiscovery, Victoria University of Wellington, Wellington, New Zealand; [13]Maurice Wilkins Centre for Molecular Biodiscovery, University of Auckland, Auckland, New Zealand; [14]School of Chemistry and Bio21 Institute of Molecular Science and Biotechnology, University of Melbourne, Parkville, Victoria, Australia; [15]Department of Natural Products Chemistry, Graduate School of Pharmaceutical Sciences, Kyushu University, Fukuoka, Fukuoka, Japan; [16]Cellular and Molecular Epigenetics Laboratory, Graduate School of Medical Life Science, Yokohama City University, Yokohama, Kanagawa, Japan; [17]Division of Physiological Chemistry and Metabolism, Graduate School of Pharmaceutical Sciences, Keio University, Minato-ku, Tokyo, Japan; [18]Molecular Microbiology/Medical Microbiology and Infection Control, Amsterdam University Medical Centers, Amsterdam, Netherlands; [19]Division of Molecular Design, Medical Institute of Bioregulation, Kyushu University, Fukuoka, Fukuoka, Japan; [20]Division of Molecular Immunology, Medical Mycology Research Center, Chiba University, Chiba, Japan.

Correspondence to Sho Yamasaki: yamasaki@biken.osaka-u.ac.jp.

et al., 2006). On the other hand, their immunostimulatory properties and host pattern recognition receptors have not yet been determined.

Among the germline-encoded innate immune receptors, C-type lectin receptors (CLRs) have recently been demonstrated to recognize various pathogen-derived glycoconjugates (Geijtenbeek and Gringhuis, 2016). Notwithstanding, it is still unclear whether CLR family members recognize steryl glucosides in *H. pylori* and, moreover, whether CLRs are involved in gastritis induction.

In the present study, we identified host CLRs for *H. pylori*–derived pathogenic metabolites that cause detrimental inflammation.

Results

H. pylori possesses immunostimulatory lipid components recognized by Mincle

To search for the immunostimulatory lipid components in *H. pylori*, we isolated a lipophilic extract, separated it into 16 fractions by high-performance TLC (HPTLC; Fig. 1 A), and assessed the ability of each fraction to stimulate bone marrow–derived dendritic cells (BMDCs). Peaked activity corresponding to the distinct spot (R_f = 0.83, chloroform/methanol/water [65:25:4, vol/vol/vol]) was found across fraction 13 to 14 (fraction 13-14) that induced DCs to produce inflammatory cytokines, such as TNF. This activity was independent of the TLR adaptor MyD88 but was completely abolished upon deletion of CARD9 or FcRγ (Fig. 1 B), suggesting that an FcRγ-CARD9–coupled immunoreceptor, including a CLR, is involved in ligand recognition and signaling. We therefore expressed several CLRs in combination with FcRγ in NFAT-GFP reporter cells and found that fraction 13-14 activated cells expressing macrophage-inducible C-type lectin (Mincle; *Clec4e*) and FcRγ; (Fig. 1, C and D). Weak activity was also detected in cells expressing macrophage C-type lectin (MCL; *Clec4d*) and FcRγ. MCL forms heterodimers with Mincle and stabilizes its expression on the cell surface (Lobato-Pascual et al., 2013; Miyake et al., 2015; Zhao et al., 2014). We thus created Mincle-CD3ζ and MCL-CD3ζ chimeras and confirmed that Mincle is a receptor that recognizes fraction 13-14 (Fig. 1 E). Consistent with its ability to activate *Myd88*$^{-/-}$ cells (Fig. 1 B), this fraction did not possess TLR2/4 ligand activity (Fig. S1 A). The production of TNF induced by fraction 13-14 was abrogated in Mincle-deficient BMDCs (Fig. 1, F–H), demonstrating the essential role of this CLR in the recognition of components in fraction 13-14. Fraction 13-14 was visualized by staining with copper acetate-phosphoric acid (lipid stain, Fig. 1 F) and orcinol (carbohydrate stain, Fig. 1 G), suggesting that this fraction contains a glycolipid.

Identification of αCAG as a noncanonical Mincle ligand

To identify its molecular components, fraction 13-14 was repurified by HPTLC (Fig. 1 I), and its dose-dependent activity was verified using reporter cells expressing Mincle (Fig. 1 J) and by binding to Mincle-Fc protein (Fig. 1 K). We then determined its chemical structure using mass spectrometry (MS) and nuclear magnetic resonance (NMR) spectroscopy. High-resolution electrospray ionization (ESI) time-of-flight (TOF) MS showed a molecular-related ion peak at *m/z* 781.5979 $[M + Na]^+$ (Fig. 1 L), suggesting a cholesteryl acyl-pyranoside such as αCAG (calculated mass, 781.5953) as a likely candidate (Hirai et al., 1995). Methanolysis of the active fraction followed by gas chromatography (GC)–MS allowed for the identification of three saturated fatty acid methyl esters (FAMEs; 14:0, 16:0, 18:0; Fig. S1 B). The presence of a cholesterol moiety was confirmed by the detection of Δ3,5-cholesterol after methanolysis (Fig. S1, B and C).

The ^{1}H-NMR spectrum of fraction 13-14 showed characteristic signals of cholesterol, α-glucopyranoside and saturated fatty acid (Fig. 1, M and N). Furthermore, extensive 2D-NMR analyses, including ^{1}H-^{1}H correlation spectroscopy, total correlation spectroscopy, heteronuclear single-quantum coherence (HSQC), and heteronuclear multiple-bond correlation (HMBC) spectroscopy, gave the main chemical moiety in fraction 13-14 as αCAG (Fig. S1 D). Taken together, these results demonstrate that the major ligand component in *H. pylori* is cholesteryl 6-*O*-tetradecanoyl-α-glucopyranoside (αCAG, C14:0; Fig. 1 N). The structure of αCAG is distinct from previously reported Mincle ligands bearing flexible lipid tails (Lu et al., 2018), as it contains a rigid and planar tetracyclic scaffold.

H. pylori extracts cholesterol from the host and adds glucose at the 3′ position using its glucosyltransferase, *Hp0421*, which is a critical first step for the synthesis of αCAG (Hirai et al., 1995; Lebrun et al., 2006). We extracted lipid components from a mutant *H. pylori* strain lacking *hp0421* gene (*H. pylori*$^{\Delta hp0421}$). The HPTLC band corresponding to αCAG was absent from *H. pylori*$^{\Delta hp0421}$, and the equivalent fraction failed to activate Mincle reporter cells (Fig. 1 O) and BMDCs (Fig. 1 P). Thus, αCAG is a dominant *H. pylori* lipid that signals through Mincle.

Immunostimulatory properties of αCAG

To verify that the activity of fraction 13-14 did not result from minor contaminants, we chemically synthesized αCAG. A synthetic sample of the major αCAG identified in *H. pylori*, C14:0, potently activated reporter cells expressing Mincle at a level comparable to the authentic ligand trehalose 6,6′-dimycolate (TDM; Fig. 2 A). Cholesteryl α-glucoside (αCG), a biosynthetic precursor of αCAG, did not possess such activity. Direct binding to Mincle was confirmed by probing plate-bound synthetic αCAG with Mincle-Ig fusion protein (Fig. 2 B). In dendritic cells (DCs), synthetic αCAG induced the secretion of inflammatory cytokines (Fig. 2 C), up-regulation of costimulatory molecules (Fig. 2 D), and induction of nitric oxide synthase type 2 (NOS2; Fig. 2 E) through Mincle. Moreover, a comparison with TDM revealed that αCAG is the most potent ligand for human-derived Mincle (Fig. 2 F). Indeed, αCAG efficiently activated human monocyte–derived DCs (hMoDCs) to produce proinflammatory cytokine IL-8 (Fig. 2 G).

We thus analyzed the effect of αCAG on DC-mediated T cell priming. T cells from OVA-specific TCR transgenic mice were cultured with OVA-pulsed BMDCs in the presence or absence of synthetic αCAG. Antigen-specific production of IFN-γ and IL-17 was augmented in the presence of αCAG (Fig. 2 H). To evaluate T cell priming in vivo, mice were immunized with whole OVA protein along with αCAG, and recall response was examined. We

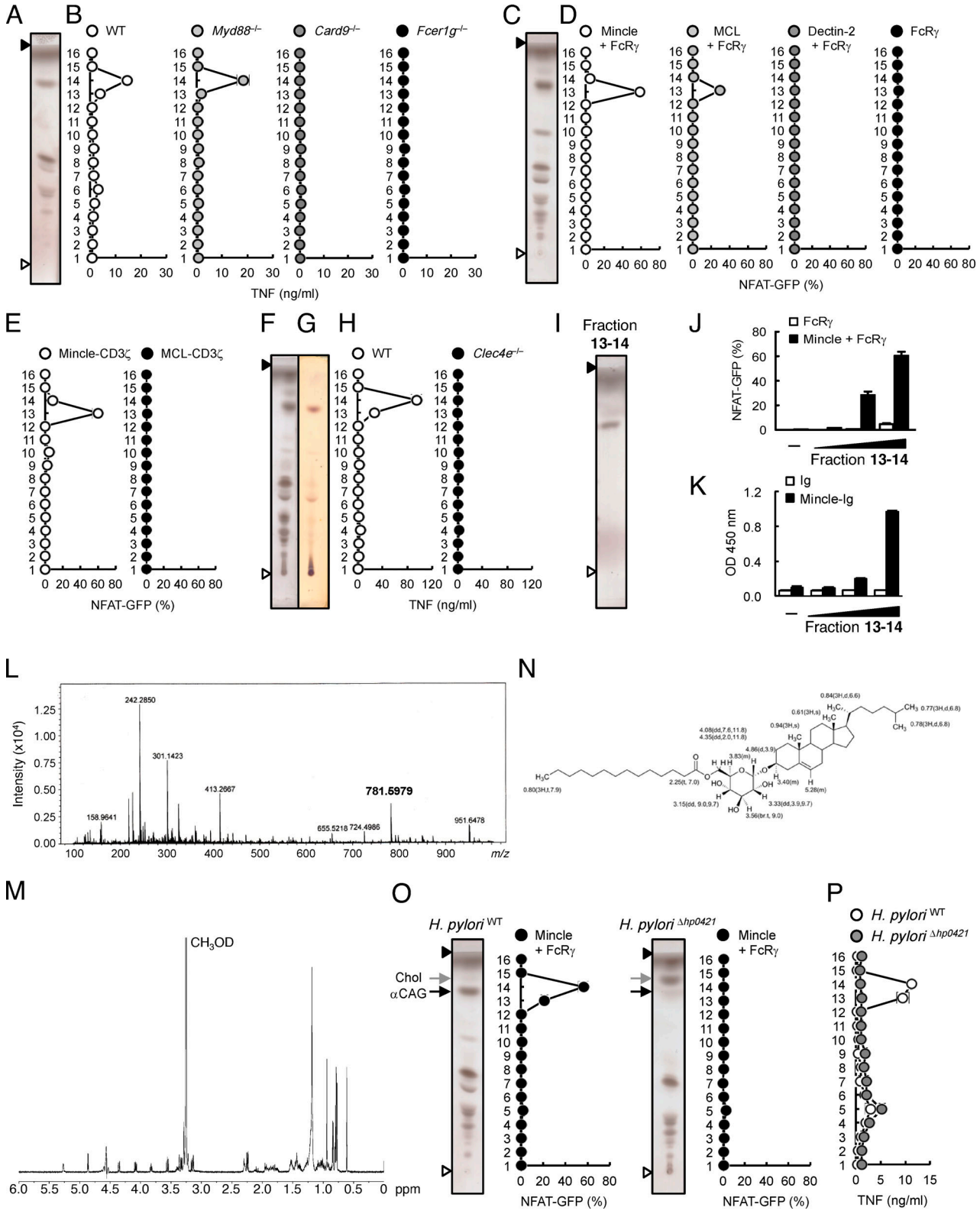

Figure 1. **Identification of αCAG as the Mincle ligand in *H. pylori*. (A, C, F, G, I, and O)** Lipid extract from *H. pylori* was analyzed by HPTLC using chloroform/methanol/water (65:25:4, vol/vol/vol) and stained with copper(II) acetate-phosphoric acid (A, C, F, I, and O) or orcinol (G). Open and closed arrowheads denote the origin and the solvent front, respectively. **(B)** BMDCs from WT, *Myd88*$^{-/-}$, *Card9*$^{-/-}$, and *Fcer1g*$^{-/-}$ mice were stimulated with HPTLC-separated fractions from *H. pylori* lipid extract for 1 d. The concentrations of TNF in the supernatants were determined by ELISA. **(D)** NFAT-GFP reporter cells expressing mouse (hereafter omitted for clarity unless needed) Mincle + FcRγ, MCL + FcRγ, Dectin-2 + FcRγ, or FcRγ alone were stimulated with HPTLC-separated fractions from *H. pylori* lipid extract for 20 h. Induction of GFP was analyzed by flow cytometry. **(E)** Mincle-CD3ζ– or MCL-CD3ζ–expressing NFAT-GFP reporter cells were stimulated by individual HPTLC-separated fractions of *H. pylori* lipid extract for 20 h. Induction of GFP was analyzed by flow cytometry. **(H)** BMDCs from WT

and *Clec4e*$^{-/-}$ mice were stimulated with HPTLC-separated lipids from *H. pylori* lipid extract for 1 d. The concentrations of TNF in the supernatants were determined by ELISA. **(I)** Fraction 13-14 was purified by HPTLC using chloroform/methanol/water (65:25:4, vol/vol/vol) and visualized by copper(II) acetate-phosphoric acid staining. **(J)** Reporter cells expressing Mincle + FcRγ or FcRγ alone were stimulated by fraction 13-14 (0.01, 0.1 and 1 µg/well) for 20 h and analyzed for GFP expression. **(K)** Human Ig or Mincle-Ig was incubated with plate-coated fraction 13-14 (0.01, 0.1, and 1 µg/well). Bound proteins were detected with anti-human IgG-HRP. **(L)** Full-scan MS spectra of fraction 13-14 in the positive ion mode. Ion peak at *m/z* 781.5979 $[M + Na]^+$ is assigned as cholesteryl acyl-pyranoside (calculated mass, 781.5953). **(M)** ^{1}H-NMR (600 MHz, $CDCl_3$:CD_3OD [1:1], 298 K) spectrum of fraction 13-14. **(N)** Chemical structure and ^{1}H-NMR chemical shifts assignment of fraction 13-14. Chemical shifts are given in δ ppm, followed by integration, multiplicity, and *J* in hertz. **(O)** Reporter cells expressing Mincle + FcRγ were stimulated by HPTLC-separated lipids from WT (*H. pylori*^{WT}) or *Hp0421*-deficient *H. pylori* (*H. pylori*$^{\Delta hp0421}$) for 20 h and analyzed for GFP expression. The black arrow indicates αCAG, and the gray arrow indicates cholesterol (Chol). **(P)** WT BMDCs were stimulated for 1 d with lipid subfractions from *H. pylori*^{WT} or *H. pylori*$^{\Delta hp0421}$ as in O. The concentrations of TNF in the supernatants were determined by ELISA. Data are presented as the mean ± SD of triplicate (B, H, K, and P) or duplicate (D, E, J, and O) assays and representative of two (B, D, E, H, K, O, and P) or four (J) independent experiments.

detected IFN-γ production after restimulation of T cells from WT mice, whereas levels were lower in Mincle- and FcRγ-deficient mice (Fig. 2 I). Thus, the αCAG–Mincle–FcRγ axis promotes antigen-specific T cell priming through APC activation.

Pathophysiological contribution of Mincle to *H. pylori*–induced gastritis

To assess the pathophysiological consequences of an αCAG–Mincle interaction, we used a model of chronic *H. pylori* infection (Nagai et al., 2007). WT and *Clec4e*$^{-/-}$ mice were infected with *H. pylori* SS1 strain, and 6 wk after infection, *H. pylori*–specific recall responses were detected in T cells isolated from gastric LNs and Peyer's patches. The production of IFN-γ and IL-17 from these T cells was much weaker when *Clec4e*$^{-/-}$ mice were infected (Fig. 3, A and B). Nevertheless, bacterial numbers in the stomach were comparable between *Clec4e*$^{-/-}$ and WT mice (Fig. 3 C), suggesting that *H. pylori*–specific Th1/17 cell responses do not efficiently contribute to the eradication of bacteria. Chronic gastritis was observed in WT mice after infection of *H. pylori*; however, the severity of gastritis as assessed by histological analysis was ameliorated in *Clec4e*$^{-/-}$ mice (Fig. 3 D). Increased numbers of neutrophils and macrophages in stomach homogenates from infected mice was suppressed in *Clec4e*$^{-/-}$ mice (Fig. 3 E and Fig. S2, A and B). Transcriptome analysis of gastric tissue revealed that the expression of inflammatory gene sets was significantly lower in *Clec4e*$^{-/-}$ mice (Fig. 3 F), further confirming that chronic gastritis was attenuated in the absence of Mincle. This effect is unlikely due to the difference of gastric microbiota in WT and *Clec4e*$^{-/-}$ mice, as assessed by metagenome analysis (Fig. S2 C). Collectively, these results indicate that Mincle contributes to *H. pylori*–induced gastritis. In line with these results, antibody (Ab) blockade of Mincle resulted in the suppression of T cell responses (Fig. 3, G–I; and Fig. S2 D) and chronic gastritis (Fig. 3 J and Fig. S2 E) without increasing the number of *H. pylori* (Fig. 3 K).

Nontargeting lipidomics reveals inflammatory conversion of *H. pylori* metabolites

Helical *H. pylori* bacilli in the stomach transform into dormant coccoid forms under anaerobic conditions, such as in the small intestine and Peyer's patches (Noach et al., 1994). As previous studies revealed that the coccoid form has more potent immunostimulatory activity, we reproduced this transformation in vitro under anaerobic culture (Fig. 4 A; Nagai et al., 2007). Extracts from helical and coccoid forms were subjected to lipidomic analysis using liquid chromatography coupled with quadrupole/TOF MS (Tsugawa et al., 2020). Nontargeted lipidomics revealed that the lipid composition was markedly altered by the helical/coccoid conversion, particularly for cholesterol-containing lipids (Fig. 4 B), although cholesterol ester species were mostly unchanged (Fig. S3, A and B). TLC analysis also confirmed the alteration of lipid composition, with the most prominent changes being the band shift of αCAG (Fig. 4 C, black arrow) and the appearance of newly generated lipids in coccoid form (Fig. 4 C, gray arrow; designated as Spot-specific for coccoid form [Spot C]). Analysis of the molecular composition of αCAG revealed that longer fatty acids that were trace components in helical form became abundant in the coccoid form (Fig. 4 D and Fig. S3 C); correspondingly short-chain myristate (C14:0) αCAG decreased in coccoid form. We therefore synthesized αCAG with different fatty acids, myristate (C14:0), palmitate (C16:0), and stearate (C18:0) and found that the activity of αCAG increased as their fatty acyl chains were elongated, as assessed by production of inflammatory cytokines (Fig. 4, E–G) and using reporter cells expressing Mincle (Fig. 4 H).

As described above, the amount of a polar glycolipid, Spot C, that was visualized by orcinol staining was markedly increased in coccoid form (Fig. 4 C, Spot C). When peritoneal macrophages were stimulated with Spot C, IL-6 production was detected in a CARD9-dependent manner (Fig. 4 I). Since Spot C was not recognized by Mincle, we tested several receptors and identified DC immunoactivating receptor (DCAR; *Clec4b1*; Fig. 4 J), an FcRγ-coupled CLR, as the candidate receptor. DCAR is known to recognize acylated phosphatidylinositol mannosides (AcPIMs) in mycobacteria (Toyonaga et al., 2016). However, as *H. pylori* does not possess AcPIM species (Tannaes et al., 2000), DCAR must recognize a previously unappreciated ligand in *H. pylori*. Using ESI-quadrupole Orbitrap MS (ESI-Q-Orbitrap-MS; Fig. 4, K and L; and Fig. S4, A and B), methanolysis followed by GC-MS (Fig. S4, C and D), and NMR spectroscopic analysis (Fig. 4, M and N; and Fig. S4 E), Spot C was identified as cholesteryl phosphatidyl α-glucoside (αCPG; Fig. 4 N). Lipidomics data targeted on αCPG revealed that the relative amount of αCPG was markedly increased in the coccoid form as observed on TLC (Fig. 4 C), whereas in contrast to αCAG, its fatty acid composition was unchanged (Fig. 4 O and FFig. S3 D). αCPG is distinctive in structure from known DCAR ligands AcPIMs (Toyonaga et al., 2016), except that both share a phosphate-containing phosphatidyl group. We thus synthesized αCPG and an αCPG

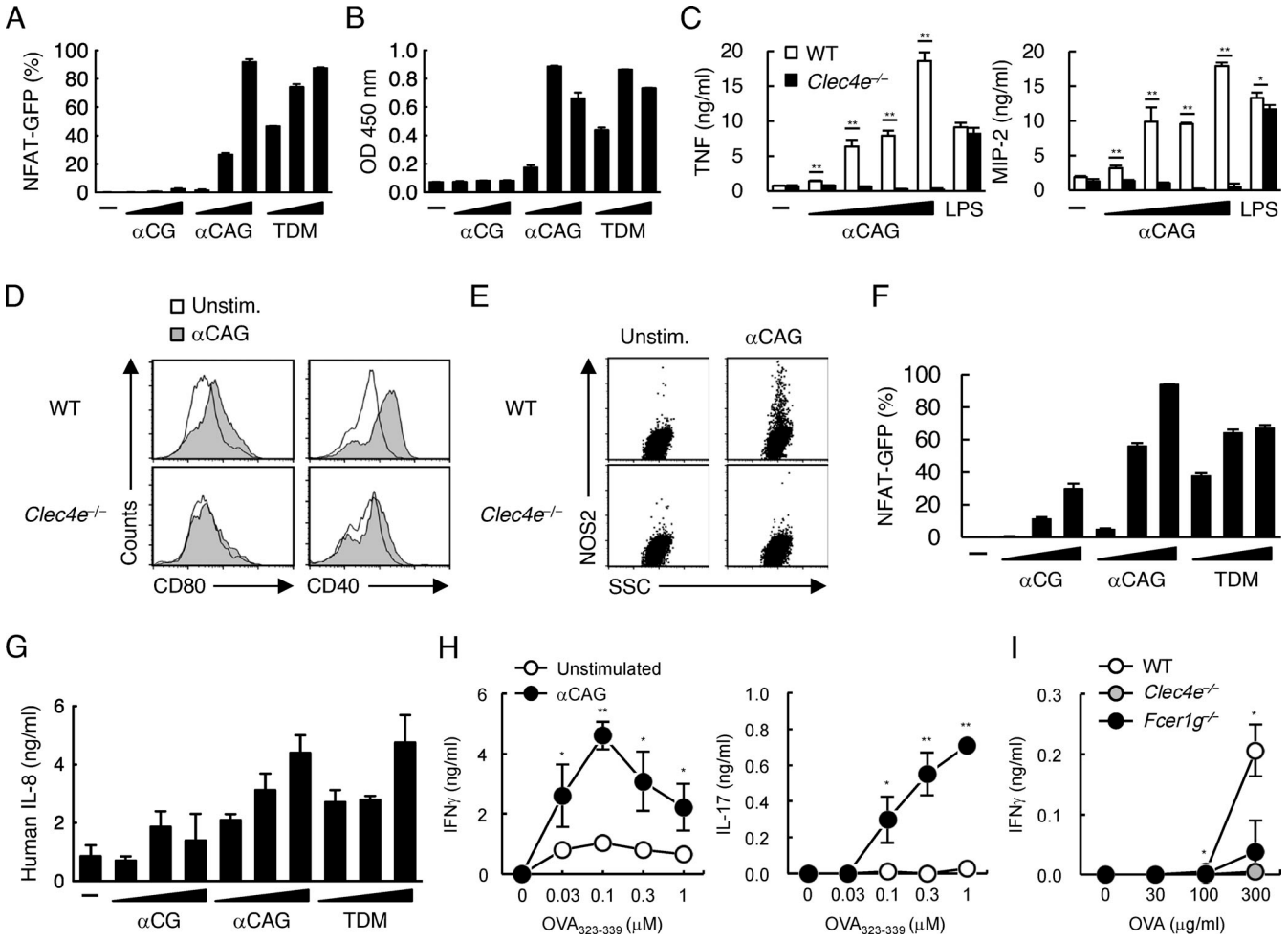

Figure 2. **αCAG induces innate and acquired immune responses as potent as TDM. (A)** Reporter cells expressing Mincle + FcRγ were stimulated with αCG, αCAG C14:0, or TDM (0.003, 0.03, and 0.3 nmol/well) for 20 h and analyzed for GFP expression. **(B)** Binding of Mincle-Ig to plate-coated αCG, αCAG C14:0, or TDM (0.001, 0.01 and 0.1 nmol/well). Bound proteins were detected with anti-human IgG-HRP. **(C)** WT and *Clec4e*$^{-/-}$ BMDCs were stimulated with αCAG C14:0 (0.001, 0.01, 0.1, and 1 nmol/well) or LPS for 1 d and cytokine production was quantified. **(D)** WT and *Clec4e*$^{-/-}$ BMDCs were stimulated with αCAG C14:0 for 1 d and analyzed for the surface expression of CD80 and CD40. **(E)** IFN-γ–primed BMDCs were stimulated with αCAG C14:0 for 1 d and analyzed for the expression of intracellular NOS2. SSC, side scatter. **(F)** Reporter cells expressing human Mincle + FcRγ were stimulated with αCG, αCAG C14:0, or TDM (0.003, 0.03, and 0.3 nmol/well) and analyzed for GFP expression. **(G)** hMoDCs were stimulated with αCG, αCAG C14:0 or TDM (0.04, 0.1, and 0.3 nmol/well) for 1 d, and IL-8 production was quantified. **(H)** BMDCs were stimulated with 0.1 nmol/well of αCAG C14:0, and co-cultured with OT-II CD4^{+} T cells in the presence of $OVA_{323–339}$ peptide for 3 d. Cytokine concentrations were measured by ELISA. **(I)** Mice were immunized with OVA + αCAG C14:0 and challenged with heat-aggregated OVA at 7 d after immunization. At day 7 after OVA challenge, B cell–depleted inguinal LN cells were stimulated with indicated amounts of OVA for 4 d, and IFN-γ production was quantified. The results of the statistical analysis show the difference between WT and *Clec4e*$^{-/-}$ mice. Data are presented as the mean ± SD of triplicate (B, C, G, and H) or duplicate (A, F, and I) assays and representative of three (A, B, F, and H), five (C and D), two (E and I), or four (G) independent experiments. An unpaired two-tailed Student's *t* test was used for the statistical analyses. *, P < 0.05; **, P < 0.01.

analogue lacking the phosphate moiety, cholesteryl amide-linked α-glucoside (Fig. S4 F). Synthetic αCPG, but not the amide analogue, signaled through DCAR (Fig. 4 P), suggesting that phosphate is a key structural feature for DCAR binding which is absent in αCAG.

Depletion of αCAG/αCPG in *H. pylori* impairs its virulence

To examine the contribution of αCAG/αCPG to host responses against *H. pylori*, we investigated the immunostimulatory activity of mutant *H. pylori* lacking cholesterol glucosyltransferase (*H. pylori*$^{\Delta hp0421}$), which cannot generate αCAG and αCPG (Lebrun et al., 2006). We confirmed complete loss of these cholesteryl glucosides in both helical and coccoid forms of *H. pylori*$^{\Delta hp0421}$ (Fig. 5 A). The up-regulation of CD80 on the surface of BMDCs in response to *H. pylori* was impaired in this mutant strain (Fig. 5 B). Thus, *H. pylori*^{WT} and *H. pylori*$^{\Delta hp0421}$ were further evaluated for their T cell priming potential via co-culture with model antigen-pulsed DCs and OT-II T cells. The antigen-dependent secretion of IFN-γ and IL-17 from OT-II T cells was significantly lower when cultured with *H. pylori*$^{\Delta hp0421}$ compared with *H. pylori*^{WT} (Fig. 5, C and D, left panels). Reduction in cytokine secretion was similar to the suppression detected when we used FcRγ-deficient BMDCs in which Mincle and DCAR are nonfunctional (Fig. 5, C and D, right panels). However, cytokine production was restored following the addition of synthetic αCAG to *H. pylori*$^{\Delta hp0421}$

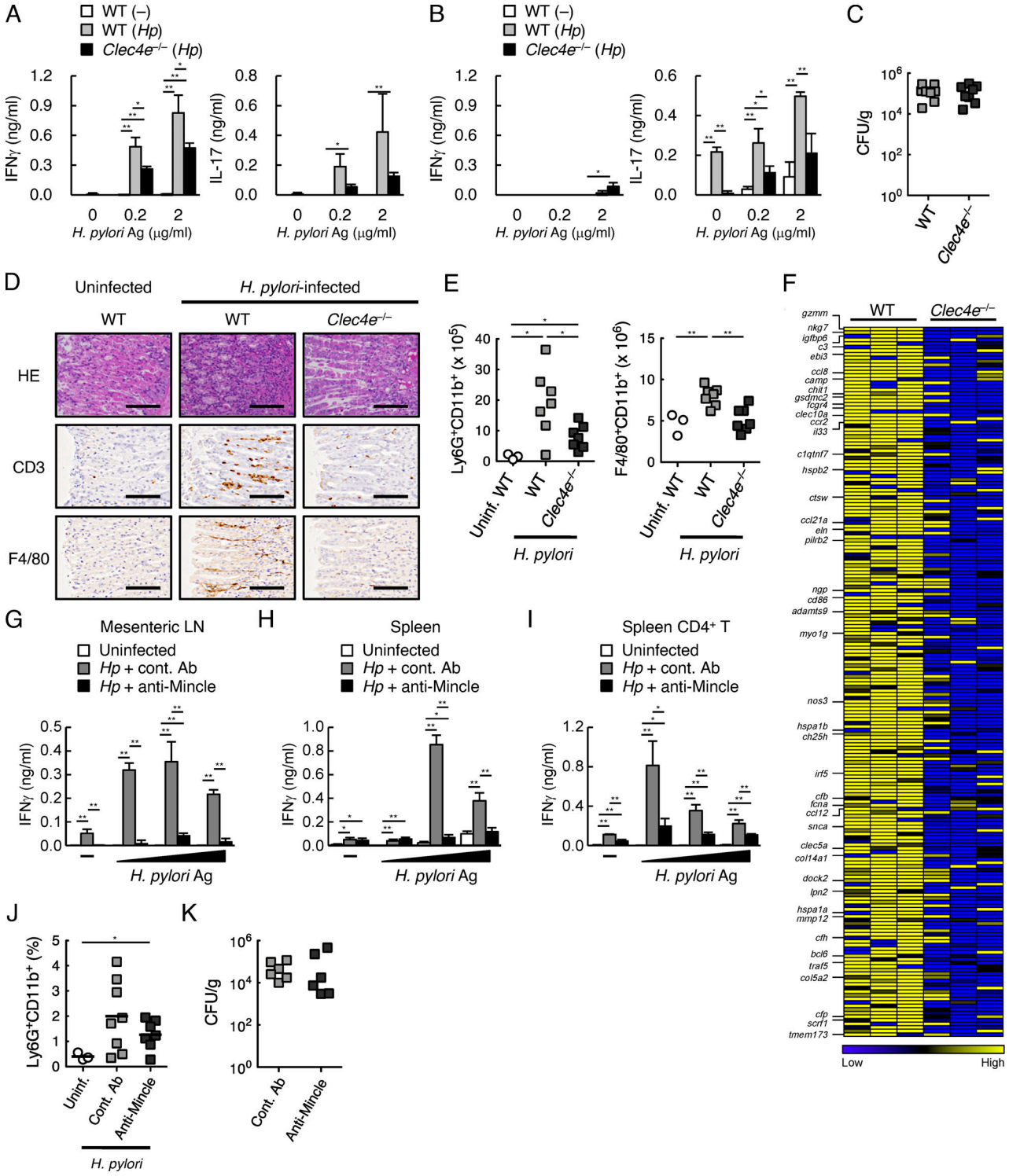

Figure 3. **Pathogenic role of Mincle in *H. pylori*–induced gastritis. (A and B)** WT or *Clec4e*$^{-/-}$ mice were orally administered with 3 × 10^8 CFU of *H. pylori* SS1 three times in 2 d. At 6 wk after infection, cells from gastric LNs (A) or Peyer's patches (B) were stimulated with indicated concentrations of *H. pylori* lysates (Ag) in the presence of BMDCs for 4 d. Uninfected WT mice were used as control. The concentrations of IFN-γ (left panel) and IL-17 (right panel) in the supernatant were determined by ELISA. **(C)** The number of bacteria recovered from the stomachs of WT and *Clec4e*$^{-/-}$ mice at 8 wk after *H. pylori* infection. Bacterial numbers were determined by counting the number of colonies on *H. pylori* selective agar plates. **(D)** H&E (HE) staining and immunohistochemical staining of anti-CD3 and F4/80 of stomach sections from uninfected and *H. pylori*–infected mice after 8 wk. Scale bar, 100 μm. **(E)** The numbers of Ly6G$^+$CD11b$^+$ or F4/80$^+$CD11b$^+$ cells in gastric MNC from mice at 6 wk after infection. **(F)** Heat map of differentially expressed genes based on RNA-sequencing analysis using RNA extracted from the stomachs of *H. pylori*–infected WT or *Clec4e*$^{-/-}$ mice (n = 3 in each group) after 8 wk. **(G–I)** *H. pylori*–infected mice were injected with anti-Mincle mAb or rat IgG as a control Ab (cont. Ab). After 8 wk, single-cell suspensions of mesenteric LN (G), spleen (H), or splenic CD4$^+$ T cells (I; in the presence of BMDCs) were stimulated with *H. pylori* lysates (2, 20, and 200 μg/ml) for 4 d. Uninfected WT mice were used as control. The concentrations

of IFN-γ in the supernatant were determined by ELISA. **(J)** The frequency of $Ly6G^+CD11b^+$ cells in gastric MNCs was analyzed at 6 wk after infection with anti-Mincle mAb or cont. Ab treatment. Bars indicate the average number. **(K)** Bacterial CFU in the stomach of infected mice was determined by counting the number of colonies on *H. pylori* selective agar plates. Littermates (A–F) or C57BL/6J mice obtained from CLEA Japan (G–K) were used as WT mice. Data are presented as the mean ± SD of triplicate assays (A, B, and G–I) from three (WT vs. *Clec4e*$^{-/-}$) or two (Control Ab vs. Anti-Mincle) independent experiments (at least six infected mice in each group) with similar results. An unpaired two-tailed Student's *t* test was used for the statistical analyses. *, P < 0.05; **, P < 0.01.

(Fig. 5, E and F), suggesting that αCAG is one of the major components of *H. pylori* responsible for T cell priming.

Finally, we addressed the role of cholesteryl glucosides in *H. pylori*–induced gastritis. Gastritis was significantly ameliorated in mice infected with *H. pylori*$^{\Delta hp0421}$ compared with *H. pylori*^{WT}, as assessed by inflammatory cell infiltration in the mucosa (Fig. 5, G and H). In contrast, bacterial numbers in the stomach were not significantly altered (Fig. 5 I). Similarly, we detected a substantial titer of anti–*H. pylori* Ab upon infection with *H. pylori*$^{\Delta hp0421}$ in WT mice, as well as *H. pylori*^{WT} in *Clec4e*$^{-/-}$ mice (Fig. 5, J and K). These results suggest that the production of cholesteryl glucosides, αCAG and αCPG, by *H. pylori* is required for its virulence to promote gastritis without affecting humoral immune responses.

Discussion

In the present study, we provide the first example of an innate immune recognition of self-lipid–derived virulence factor generated by bacterial pathogens. These immune responses did not, however, efficiently contribute to *H. pylori* clearance (Adamsson et al., 2017).

In addition to the established role of Th1 (Eaton et al., 2001), recent studies have underscored the contribution of the Th17 population for the induction and development of gastritis during *H. pylori* infection (Ericksen et al., 2014; Gray et al., 2013). In the present study, *H. pylori* lipids augmented both Th1 and Th17 responses, which is consistent with the reported characteristics of CLR signaling (Geijtenbeek and Gringhuis, 2016). Another T cell subset, invariant natural killer T (iNKT) cells, are reported to be activated by cholesteryl glucosides (Chang et al., 2011; Ito et al., 2013; Shimamura, 2012), although we did not observe detectable iNKT cell activation by αCAG and αCPG (Fig. S2 F). Alternatively, αCAG and αCPG might activate iNKT cells through macrophage/DC-derived IL-12 in a TCR-independent manner (Cohen et al., 2011). However, there was no significant difference in the phenotypes of WT mice and Jα18-deficient (*Traj18*$^{-/-}$) mice lacking iNKT cells after *H. pylori* infection (Fig. S2, G and H), suggesting that iNKT cells play a limited role in immune responses against *H. pylori* in the present SS1 model.

Some bacteria and fungi produce nonsteryl aliphatic ligands bearing flexible tails that signal through Mincle (Lu et al., 2018). *H. pylori*–derived Mincle ligand is atypical in its structure (Fig. 1 N) and recognition mode (Fig. S1 E), and the induction of gastritis is a pathology specific to *H. pylori*. Possibly, the continuous priming of APCs by rigid steroid-based ligands during chronic infection in gastric lymphoid tissues may efficiently induce pathogenic T cells. Most likely, these events take place in a less acidic environment, as the immune-active coccoid form of *H. pylori* is efficiently taken up by DCs in the duodenum or small intestine, particularly in secondary lymphoid organs (Nagai et al., 2007). Indeed, these DCs are activated in *H. pylori*–infected individuals and induce Th1 response (Bimczok et al., 2010).

αCAG is the most potent Mincle ligand in human. Although humans lack a DCAR orthologue (Flornes et al., 2004), αCPG potently activated human DCs (Fig. S4 G), indicating that αCPG may also exert their effect in humans via an unidentified receptor. Our recent report of murine DCAR–ligand complex structure (Omahdi et al., 2020) will help with the structure-based identification of human counterpart. Collectively, these results suggest that blockade of *Hp0421* may prevent gastritis in humans by reducing the level of αCAG and αCPG. Although an *H. pylori*$^{\Delta hp0421}$ mutant did not show an apparent growth disadvantage in our experimental setting, inactivation of this enzyme in other clinical strains of *H. pylori* led to impaired growth (Kawakubo et al., 2004; McGee et al., 2011), which may further provide therapeutic benefit.

αCAG and αCPG are unique to *Helicobacter* spp. (Grille et al., 2010; Haque et al., 1996; Hirai et al., 1995; Mayberry and Smith, 1983). Although the physiological advantage of cholesterol glycosylation in *H. pylori* remains to be fully understood, several beneficial roles of αCAG for the bacteria have been reported (Grille et al., 2010; McGee et al., 2011; Morey et al., 2018; Wunder et al., 2006). The function of αCPG has not been demonstrated in both bacteria and host. It is also proposed that sterol glycosylation and subsequent acylation by *H. pylori* may detoxify environmental sterols that may be harmful to bacteria (Shimomura et al., 2013).

On the other hand, the conservation of apparently disadvantageous recognition of these metabolites by the host implies that these interactions may confer other advantages to the host, although we could not observe it in the context of *H. pylori* infection. Given that Mincle plays a protective role against mycobacterial infection (Kabuye et al., 2019; Lu et al., 2018), it may have conferred a survival advantage to the host. Such a trade-off between "chronic inflammation" and "protective immunity" may provide selection pressures that could potentially alter the CLR family lineup during evolution. Indeed, some CLR members have been lost/pseudogenized or arisen by gene duplication in mammalian species (Flornes et al., 2004).

Nontargeted lipidomics allowed for the identification of uncharacterized cholesteryl lipid species in *H. pylori*. In addition to the above-mentioned "diacyl" αCPG, we detected *lyso*-type CPG C19c:0 (*lyso*-αCPG) in the coccoid form, yet its biological function remains unclear. We also identified cholesteryl glycerophosphate glycoside and cholesteryl ethanolamine-phosphate glycoside (Fig. S5), which have not been previously reported. These are potential candidates for as-yet-uncharacterized immunomodulatory metabolites.

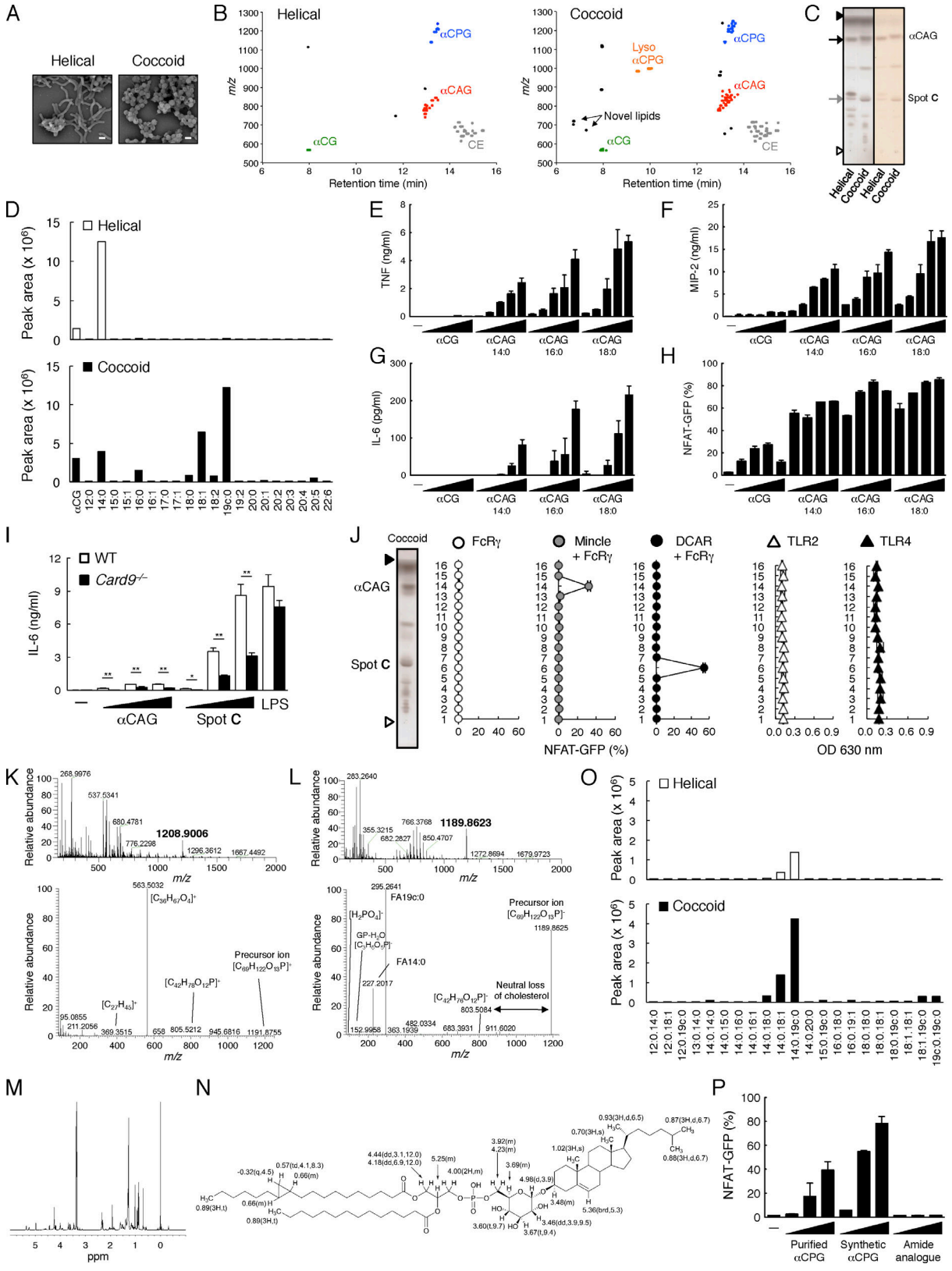

Figure 4. **Nontargeted lipidomics of *H. pylori* revealed the regulation of immunostimulatory potential by changing lipid composition. (A)** Scanning electron micrographs of helical form and coccoid form of *H. pylori*. Scale bar, 10 µm. **(B)** 2D map of mass (*m/z* of precursor ions) versus liquid chromatography retention time of cholesteryl lipids isolated from helical (left panel) or coccoid (right panel) form of *H. pylori*. Plots of precursor ions were identified as cholesterol ester (CE), αCG, αCAG, αCPG, and lyso αCPG (detected only in coccoid form). **(C)** Lipid extracts from helical or coccoid form of *H. pylori* were analyzed by HPTLC using chloroform/methanol/water (65:25:4, vol/vol/vol) and stained with copper(II) acetate-phosphoric acid (left) or orcinol (right). Open

and closed arrowheads denote the origin and the solvent front, respectively. The black arrow indicates αCAG, and the gray arrow indicates the lipid component increasing in coccoid form (Spot C). **(D)** Peak area of each fatty acid fragment ion of αCAG that is analyzed in Fig. S3 C. **(E–G)** BMDCs were stimulated with αCG, αCAG C14:0, C16:0, or C18:0 (0.02, 0.06, 0.2, 0.6, and 2 nmol/well) for 1 d. The concentrations of TNF (E), MIP-2 (F), and IL-6 (G) in the supernatants were determined by ELISA. **(H)** Reporter cells expressing Mincle + FcRγ were stimulated with αCG, αCAG C14:0, C16:0, or C18:0 (0.016, 0.08, 0.4 and 2 nmol/well) for 20 h and analyzed for GFP expression. **(I)** Resident peritoneal exudate cells from WT or *Card9*$^{-/-}$ mice were stimulated with αCAG C14:0, Spot C (0.02, 0.2, and 2 nmol/well) or LPS. IL-6 production was quantified by ELISA. **(J)** NFAT-GFP reporter cells expressing FcRγ alone, Mincle + FcRγ or DCAR + FcRγ or HEK-based NF-κB reporter cells expressing TLR2 or TLR4 were stimulated with HPTLC-separated lipids from coccoid *H. pylori* for 20 h and analyzed for GFP or SEAP expression. **(K)** Full scan MS spectra of Spot C (upper panel) and MS/MS spectra of *m/z* 1208.9006 $[M+NH_4]^+$ (lower panel) in the positive ion mode. Ion peak at *m/z* 1208.9006 $[M + NH_4]^+$ is proposed to be cholesteryl α-phosphatidylpyranoside (calculated mass, 1208.9040). **(L)** Full-scan MS spectra of Spot C (upper panel) and MS/MS spectra of *m/z* 1189.8623 $[M-H]^-$ (lower panel) in the negative ion mode. Ion peak at *m/z* 1189.8623 $[M-H]^-$ is supposed to be cholesteryl α-phosphatidylpyranoside (calculated mass, 1189.8629). **(M)** ^{1}H-NMR spectrum (600 MHz, $CDCl_3$:CD_3OD:D_2O [65:35:5], 298 K) of Spot C. **(N)** Chemical structure and ^{1}H-NMR chemical shifts assignment of Spot C. Chemical shifts are given in δ ppm, followed by integration, multiplicity and *J* in hertz. **(O)** Peak area of each fatty acid fragment ion of αCPG that is analyzed in Fig. S3 D. **(P)** Reporter cells expressing DCAR + FcRγ were stimulated with purified αCPG, synthesized αCPG (C14:0 19c:0) or αCPG amide analogue (0.1, 0.3 and 1 nmol/well) for 20 h and analyzed for GFP expression. Data are presented as the mean ± SD of triplicate (E–G and I) or duplicate (H, J, and P) assays and are representative of two independent experiments. An unpaired two-tailed Student's *t* test was used for the statistical analyses. *, P < 0.05; **, P < 0.01.

Clinical studies have demonstrated that a low vitamin D concentration is correlated with severe gastritis and that vitamin D administration attenuated *H. pylori* infection and decreased gastritis; however, the molecular basis remains unclear (Antico et al., 2012; Hosoda et al., 2015; Kawamura et al., 2006). Vitamin D3 is a 3β-OH steroid that is efficiently assimilated by *H. pylori* (Shimomura et al., 2013), implying that one of the molecular mechanisms of the effect of vitamin D is through its action as a competitive inhibitor of *Hp0421*. Development of vitamin D derivatives that inhibit this enzyme might provide a harmless regimen for the prevention of *H. pylori*–induced gastritis and subsequent malignancy.

Antibiotic eradication of *H. pylori* is an established therapy to prevent *H. pylori*–induced gastritis. Recently, however, such methods are limited due to the emergence of drug resistance and microbial dysbiosis (Labenz, 2001; Wu et al., 2012). Furthermore, incomplete treatment with antibiotics increases the risk of accelerating gastritis through induction of the coccoid form (Poursina et al., 2013). Therefore, targeting *Hp0421* or conversely the innate immune receptors for its products may provide a complementary approach to current antibiotic treatments. *Helicobacter*-specific T helper cells are also implicated in the pathophysiology of hematopoietic diseases such as mucosa-associated lymphoid tissue lymphoma and idiopathic thrombocytopenia purpura (D'Elios et al., 2005; Frydman et al., 2015), which can be addressed in mice using clinical isolates of *Helicobacter* spp. (Matsui et al., 2014). Thus, the identification of host lipid-derived bacterial adjuvants and their host receptors that drive T cell activation is potentially of broad clinical significance.

Materials and methods

Mice

Mincle-deficient mice (Yamasaki et al., 2009) were backcrossed for at least 16 generations with C57BL/6. FcRγ-deficient mice (Park et al., 1998) were provided by T. Saito (RIKEN, Yokohama, Japan). CARD9-deficient mice (Hara et al., 2007) were provided by H. Hara (Kagoshima University, Kagoshima, Japan). MyD88-deficient mice (Adachi et al., 1998) were purchased from Oriental Yeast. Jα18-deficient mice (Cui et al., 1997) were provided by M. Taniguchi (RIKEN, Yokohama, Japan). OVA-specific TCR OT-II transgenic mice (Barnden et al., 1998) were used on a C57BL/6 background. All mice were maintained in a filtered-air laminar-flow enclosure and given standard laboratory food and water ad libitum. All animal protocols were approved by the committee of Ethics on Animal Experiment, Faculty of Medical Sciences, Kyushu University and Research Institute for Microbial Diseases, Osaka University.

Reagents

TDM and αCG were purchased from Sigma-Aldrich. Synthetic αCAG, αCG, αCPG, and αCPG analogue were synthesized as described below. Anti-CD11b (M1/70), Ly6G (1A8), B220 (RA3-6B2), and CD40 (3/23) mAbs were from BD Biosciences. Anti-CD80 (16-10A1), TCR-β (H57), and CD69 (H1.2F3) mAbs were from BioLegend. Anti-F4/80 (BM8) and NOS2 (CXNFT) mAbs were from eBioscience. Anti-Mincle (1B6) mAb was from MBL. For histological analysis, anti-CD3 (A0452) Ab and F4/80 (Cl:A3-1) mAb were from Dako and AbD Serotec, respectively. The ELISA kits for TNF, IL-6, and IFN-γ were from BD Biosciences. The ELISA kits for MIP-2, IL-17, and human IL-8 were from R&D Systems and Invitrogen, respectively.

Cells

2B4-NFAT-GFP reporter cells expressing murine CLRs and human Mincle were prepared as previously described (Kiyotake et al., 2015; Miyake et al., 2013; Toyonaga et al., 2016; Yamasaki et al., 2008; Yonekawa et al., 2014). HEK293-derived reporter cells that stably express an NF-κB–inducible secreted embryonic alkaline phosphatase (SEAP) reporter gene and TLR2 or TLR4 gene were obtained from InvivoGen. BMDCs and hMoDCs were prepared as previously described (Kiyotake et al., 2015; Nagata et al., 2017). DN32.D3 (Lantz and Bendelac, 1994) cells were provided by Y. Kinjo (Jikei University School of Medicine, Tokyo, Japan).

Bacteria

The *H. pylori* strain SS1, a mouse-adapted human isolate, was used for all the experiments. The *Hp0421*-deficient SS1 strain (*H. pylori*$^{\Delta hp0421}$) was described previously (Chang et al., 2011). Glycerol stocks of *H. pylori* SS1 were first grown on 5% sheep blood agar plates (BBL: 251239) under microaerobic conditions

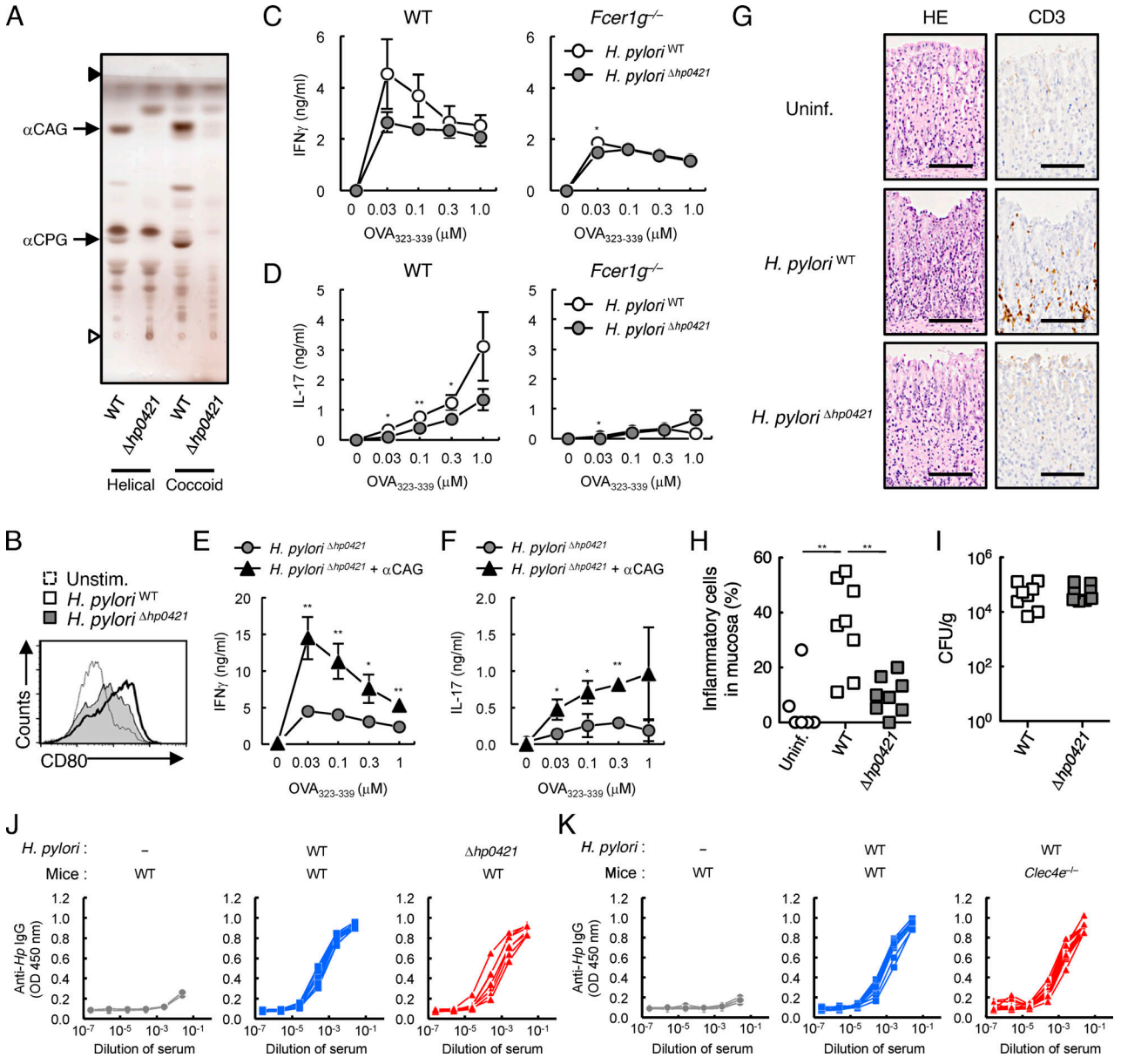

Figure 5. **Ameliorated gastritis by depletion of αCAG/αCPG in *H. pylori*. (A)** The lipid extracts from helical or coccoid form of *H. pylori*^{WT} or *H. pylori*$^{\Delta hp0421}$ were analyzed by HPTLC. Open and closed arrowheads denote the origin and the solvent front, respectively. The black arrows indicate αCAG and αCPG. **(B)** BMDCs were stimulated with multiplicity of infection (MOI) 30 of *H. pylori*^{WT} or *H. pylori*$^{\Delta hp0421}$ for 1 d, and the surface expression of CD80 was analyzed. **(C and D)** WT or *Fcer1g*$^{-/-}$ BMDCs were stimulated with MOI 30 (C) or 100 (D) of *H. pylori*^{WT} or *H. pylori*$^{\Delta hp0421}$ and co-cultured with OT-II CD4$^+$ T cells in the presence of indicated concentrations of $OVA_{323-339}$ peptide for 3 d. IFNγ (C) and IL-17 (D) productions were quantified by ELISA. **(E and F)** BMDCs were stimulated with *H. pylori*$^{\Delta hp0421}$ (MOI 30 in E or MOI 100 in F) alone or with 0.1 nmol/well of αCAG (C14:0) and co-cultured with OT-II CD4$^+$ T cells. Cytokine production was quantified as in C and D. **(G)** H&E (HE) staining and immunohistochemical staining of anti-CD3 of stomach sections from *H. pylori*^{WT}– or *H. pylori*$^{\Delta hp0421}$-infected mice at 8 wk after infection. Uninfected WT mice were used as control. Scale bar, 100 μm. **(H)** The percentage of microscopic fields with inflammatory cells in one section of gastric mucosa. Two H&E-stained sections (14–25 fields) per mice were analyzed. **(I)** The number of bacteria recovered from the stomachs of *H. pylori*^{WT}– or *H. pylori*$^{\Delta hp0421}$–infected mice. Bacterial numbers were determined by counting the number of colonies on *H. pylori* selective agar plates. **(J and K)** Production of *H. pylori*–specific Ab in the sera of *H. pylori*^{WT}– or *H. pylori*$^{\Delta hp0421}$–infected WT mice (J), and *H. pylori*^{WT}–infected WT or *Clec4e*$^{-/-}$ mice (K). *H. pylori*–specific IgG was detected by ELISA using *H. pylori* lysate as an antigen. Each line represents an individual mouse. C57BL/6J mice obtained from CLEA Japan, Inc. were used as WT mice (G–I). Data are presented as the mean ± SD of triplicate assays (C–F) and representative of two independent experiments. An unpaired two-tailed Student's *t* test was used for the statistical analyses. *, $P < 0.05$; **, $P < 0.01$.

for 2 d. After the plate culture, *H. pylori* SS1 was grown in Brucella broth (BD Biosciences) with 5% FCS for 14–16 h at 37°C under microaerobic conditions with gentle agitation. For the preparation of the coccoid form, SS1 was incubated in Brucella broth with 5% FCS for 2–3 d under anaerobic conditions after the microaerobic liquid culture or on 5% sheep blood agar plates for 7 d under anaerobic conditions after the first growth on the agar plates for 3 d.

Lipid extraction and purification

H. pylori was washed with PBS and then treated with chloroform/methanol (2:1, vol/vol) for 1 d. This mixture was partitioned by

centrifugation and the lower organic phase was used as the lipid extract. To isolate αCAG or αCPG, the lipid extracts were separated by HPTLC (Merck) and visualized by copper(II) acetate-phosphoric acid (180°C, 15 min) or orcinol (120°C, 5–15 min) staining. The fractions containing these lipids were scraped from the plate, and chloroform/methanol (2:1, vol/vol) was used to elute the lipids. The purified lipids were filtered using Millex-LG (0.2 µm; Merck) to remove silica gel contamination.

ESI-TOF-MS and GC-MS analysis of αCAG and αCPG

ESI-TOF-MS was measured with a Bruker micro-TOF mass spectrometer in the positive ESI mode (Bruker Daltonics). For conversion to FAMEs for GC-MS analysis, αCAG from the helical form of *H. pylori* was subjected to methanolysis by heating with 10% HCl/methanol in a sealed tube at 80°C for 3 h. The reaction mixture was diluted with methanol and extracted with *n*-hexane. The *n*-hexane extract was concentrated in vacuo to give a mixture of FAMEs. The FAMEs were dissolved in acetone and subjected to GC-MS with GC-MS-QP2010 SE (Shimadzu). The conditions of GC-MS were as follows: column, INERTCAP 5MS/SIL (0.25 mm i.d. × 30 m; GL Science); column temperature, 100–280°C; rate of temperature increase, 18°C/min. Three major FAMEs were detected and the retention time (t_R), and the proportions (%) of each FAME of αCAG were as follows: methyl tetradecanoate (14:0), t_R [min] = 12.3, 35.4%; methyl palmitate (16:0), t_R [min] = 14.5, 6.7%; methyl stearate (18:0), t_R [min] = 16.6, 5.8%. Dehydro cholesterol was also detected: Δ3,5-cholesterol, 41.4%, t_R [min] = 24.4, *m/z* = 368 (M^+). FAMEs of αCPG: methyl tetradecanoate (14:0), t_R [min] = 12.3, 20.4%; methyl palmitate (16:0), t_R [min] = 14.5, 3.0%; methyl octadecenoate (18:1), t_R [min] = 16.4, 3.7%; methyl stearate (18:0), t_R [min] = 16.6, 11.1%; methyl nonadecanoate, t_R [min] = 18.1, 14.3%; methyl 11,12-methyleneoctadecanoate (19c:0), t_R [min] = 19.0, 4.9%; methyl nonadecanoate (19:1), t_R [min] = 19.4, 1.9%; dehydrocholesterol was also detected: Δ3,5-cholesterol, t_R [min] = 24.4, 29.2%.

ESI-Q-Orbitrap-MS analysis of αCPG

Lipid fractions were dissolved in 5 mM ammonium acetate (wt/vol) in methanol/water (95:5, vol/vol; 50 µg/ml). Flow injection analysis was performed using a Dionex Ultimate 3000 RSLC system (Thermo Fisher Scientific) coupled with a Q Exactive, a high-performance benchtop Q-Orbitrap-MS, fitted with an ESI ion source (Thermo Fisher Scientific). The flow injection conditions in the positive and negative ionization modes were as described previously (Nagata et al., 2017).

NMR analysis of αCAG and αCPG

^{1}H- and ^{13}C-NMR spectra were recorded on an Agilent INOVA 600 spectrometer. The conditions for αCAG were as follows: ^{1}H: 600 MHz, $CDCl_3/CD_3OD$ (1:1, vol/vol), 298 K and ^{13}C: 150 MHz, $CDCl_3/CD_3OD$ (1:1, vol/vol), 298 K. The conditions for αCPG were as follows: ^{1}H: 600 MHz, $CDCl_3/CD_3OD/D_2O$ (65:35:5, vol/vol/vol), 298 K and ^{13}C: 150 MHz $CDCl_3/CD_3OD/D_2O$ (65:35:5, vol/vol/vol), 298 K. ^{1}H chemical shifts were assigned by ^{1}H-^{1}H correlation spectroscopy and total correlation spectroscopy experiments and ^{13}C chemical shifts were assigned by HSQC and HMBC experiments.

Chemical synthesis

CG and CAGs were synthesized in a multistep route as follows. Glycosylation of cholesterol using 3,4,6-tri-*O*-acetyl-2-*O*-benzyl-α-D-glucopyranosyl *N*-phenyltrifluoroacetimidate afforded cholesteryl 3,4,6-tri-*O*-acetyl-2-*O*-benzyl-α-D-glucopyranoside. Transfer hydrogenolysis of the benzyl groups (cyclohexene, $Pd(OH)_2/C$, ethanol) and then deacetylation (NaOMe, methanol/THF) afforded αCG. Trimethylsilylation (TMSCl, Et_3N, CH_2Cl_2) of αCG yielded cholesteryl 2,3,4,6-tetra-*O*-trimethylsilyl-α-D-glucopyranoside. Removal of the primary trimethylsilyl group (NH_4OAc, CH_2Cl_2/methanol) and acylation with myristoyl, palmitoyl, or stearoyl chloride (DMAP, pyr/CH_2Cl_2) afforded the cholesteryl 6-*O*-acyl-2,3,4-tri-*O*-trimethylsilyl-α-D-glucopyranosides. Finally, treatment with Dowex 50 (H^+ form) resin in methanol/CH_2Cl_2 provided αCAG-C14:0, αCAG-C16:0, and αCAG-C18:0. Natural αCPG was chemically synthesized as below. First, a common αCG derivative having a single hydroxyl group at the C6 position of glucose residue was prepared based on an in situ anomerization method to form an α-glucoside linkage. The conversion of penta-*O*-trimethylsilyl-D-glucose into the corresponding glucosyl iodide followed by the coupling with cholesterol afforded the desired cholesteryl glucoside as a mixture of diastereoisomers. Subsequent four-step reaction sequence, including the removal of TMS groups, C6-protection by the trityl group, the introduction of the Fmoc group to other hydroxyl groups, and the removal of the trityl group, gave the αCG derivative in pure form. Glycerol moiety found in natural αCPG was prepared starting from commercially available L-(−)-1,2-isopropylideneglycerol. The coupling of the glycerol derivative and myristic acid in the presence of *N*,*N*′-dicyclohexylcarbodiimide and 4-dimethylaminopyridine followed by the removal of the isopropylidene group afforded the diol product. The primary alcohol was then protected as a trityl ether. The introduction of phytomonic acid to the remaining secondary alcohol and subsequent removal of the trityl group by hydrogenolysis provided the desired glycerol unit used for natural αCPG in good yields. The prepared glycerol unit was treated with 2-cyanoethyl *N*,*N*,*N*′,*N*′-tetraisopropylphosphoroamidite and 1*H*-tetrazole to form the corresponding phosphoroamidite derivative, which was then subjected to the phosphoroamidite coupling reaction with the above-mentioned αCG derivative. The coupling successfully yielded the corresponding fully protected target framework. Finally, global deprotection delivered natural αCPG. On the other hand, the amide-linked αCPG analogue was chemically prepared via 15 reaction steps starting from the commercially available D-glucose pentaacetate. First, D-glucose pentaacetate was converted into phenyl 4,6-*O*-di-*tert*-butylsilylene-2,3-di-*O*-*p*-methoxybenzyl-1-thio-β-D-glucopyranoside as the glycosyl donor in six steps. The coupling of the glucosyl donor and cholesterol in the presence of dimethyl(methylthio)sulfonium triflate and 2,4,6-tri-*tert*-butylpyrimidine in dichloromethane at room temperature followed by the removal of the DTBS group of the glucose moiety afforded the 4,6-dihydroxy α-glucosyl

cholesterol derivative. Subsequent Mitsunobu reaction with phthalimide, 1,2-bis(diphenylphosphino)ethane, and bis(2-methoxyethyl) azodicarboxylate installed an imide functionality at the C6 position of the glucose. The 6-phthalimide derivative obtained was then transformed into the 6-NH_2 glucosyl cholesterol having *tert*-butyldimethylsilyl groups at O2, O3, and O4 positions of the glucose. The prepared 6-NH_2 glucosyl cholesterol derivative was condensed with the same glycerol unit as that used for natural αCPG in the presence of *N*,*N*′-disuccinimidyl carbonate and triethylamine, giving the fully protected amide-linked αCPG framework in good yield. Finally, the removal of *tert*-butyldimethylsilyl groups by the action of tetra-*n*-butylammonium fluoride furnished the amide-linked αCPG analogue.

In vitro stimulation assay

To stimulate the cells, each lipid was diluted in isopropanol and the 20 µl dilutions were added to each well of the 96-well plate followed by evaporation of the solvent. LPS (10 ng/ml) was used as a positive control. The reporter activity of 2B4-NFAT-GFP cells was analyzed by flow cytometry and SEAP secretion from HEK293-based NF-κB cells were detected using an alkaline phosphatase detection reagent (QUANTI-Blue; InvivoGen).

In vitro Mincle binding assay

The Mincle-Ig protein, composed of the C-terminus of the extracellular domain of Mincle fused to the N-terminus of the human IgG1 Fc region (hIgG1), was prepared as described previously (Miyake et al., 2013). For the in vitro binding assay, 3 µg/ml hIgG1-Fc (Ig) and Mincle-Ig diluted in binding buffer (20 mM Tris-HCl, 150 mM NaCl, 1 mM $CaCl_2$, and 2 mM $MgCl_2$, pH 7.0) were incubated with plate-coated glycolipids. The bound proteins were detected with anti-hIgG-HRP followed by the addition of a colorimetric substrate. Peroxidase activity was measured using the UV/Vis spectrophotometer.

Co-culture of OT-II $CD4^+$ T cells and BMDCs

BMDCs were stimulated with *H. pylori*, plate-coated αCAG, or both during this assay. OT-II $CD4^+$ T cells were sorted by CD4 microbeads (Miltenyi Biotec) from single-cell suspensions of spleen and inguinal LNs from OT-II mice. Sorted OT-II $CD4^+$ T cells were co-cultured with BMDCs at the ratio of 10:1 for 3 d in the presence of $OVA_{323–339}$ peptide.

Immunization

Mice were sensitized by a subcutaneous injection with 200 µg OVA in oil-in-water emulsion (mineral oil/Tween-80/PBS [9:1:90, vol/vol/vol]) containing 100 µg αCAG. At day 7, mice were challenged by an injection of 200 µg heat-aggregated OVA (70°C, 1 h) in 20 µl PBS into both footpads. For the in vitro restimulation analysis, at 7 d after the challenge, B cell–depleted inguinal LN cells were stimulated with the OVA protein for the indicated periods.

Bacterial infection

H. pylori SS1 were prepared from plate and liquid cultures. Mice were orally administered 3×10^8 CFUs of *H. pylori* SS1 in 400 µl of 5% FCS/Brucella broth three times in a week. For the anti-Mincle (1B6) mAb administration, mice were intravenously injected with 100 µg anti-Mincle mAb or control rat IgG twice a week for 4 wk. After the indicated time period, mice were sacrificed, and gastric LNs were collected before harvesting other tissues. Half of the stomachs were fixed with 10% formalin for 24 h and embedded in paraffin. Specimens were stained with H&E or taken for immunohistochemical analysis with anti-CD3 and F4/80 Abs. The remainder was used for the preparation of gastric mononuclear cells (MNCs) and RNA and the calculation of bacterial CFUs. The CFU was determined by plating serial dilutions of the stomach homogenates onto *H. pylori* selective agar plates (NISSUI) and counting colonies.

Preparation of gastric MNCs

Mouse stomachs were minced into small pieces and treated with 3 mM EDTA. After treatment, small pieces of stomach were digested with 250 µg/ml collagenase II (Sigma-Aldrich) and 100 µg/ml DNaseI (Roche) for 30 min at 37°C. Gastric MNCs were purified by Percoll density gradient centrifugation.

Recall responses after infection

Gastric LNs, Peyer's patches, mesenteric LNs, and spleens were collected from *H. pylori*–infected mice. These tissues were homogenized, and then single-cell suspensions were stimulated with *H. pylori* lysate in the presence or absence of WT BMDCs (tissue cells/BMDCs = 10:1). $CD4^+$ T cells were sorted by CD4 microbeads from splenocytes.

Preparation of *H. pylori* lysate

H. pylori SS1 was grown on 5% sheep blood agar plates under microaerobic conditions for 3 d and was sequentially incubated on 5% sheep blood agar plates under anaerobic condition for 7 d. After cultures, *H. pylori* SS1 were collected and sonicated in PBS. The supernatants after centrifugation were collected and used as the whole lysate of *H. pylori*. The protein concentration of the filtered whole lysate was determined using the Protein Assay Bicinchoninate Kit (Nacalai Tesque).

RNA sequencing

Total RNA was extracted from the stomachs with Sepasol-RNA I Super G (Nacalai Tesque) according to the manufacturer's instructions. Library preparation was performed using a TruSeq stranded mRNA sample prep kit (Illumina) according to the manufacturer's instructions. Whole-transcriptome sequencing was applied to the RNA samples by using an Illumina HiSeq 2500 platform in a 75-base single-end mode. The Illumina Casava ver.1.8.2 software was used for base calling. Sequenced reads were mapped to the mouse reference genome sequences (mm10) using TopHat ver. 2.0.13 in combination with Bowtie2 ver. 2.2.3 and SAMtools ver. 0.1.19. The number of fragments per kilobase of exon per million mapped fragments was calculated using Cufflinks ver. 2.2.1. The transcriptome RNA-sequencing datasets have been deposited to the National Center for Biotechnology Information Gene Expression Omnibus database under the accession number GSE136203.

16S rRNA gene sequencing of gastric microbiota

Gastric mucosal swabs were collected from uninfected WT mice, *H. pylori*–infected WT mice, and *Clec4e*$^{-/-}$ mice for 12 wk. Bacterial DNA was extracted from swab samples using a DNeasy PowerSoil Pro kit (Qiagen). Each library was prepared according to the Illumina 16S Metagenomic Sequencing Library Preparation Guide with primer set 27Fmod: 5′-AGRGTTTGATCMTGGCTCAG-3′ and 338R: 5′-TGCTGCCTCCCGTAGGAGT-3′ targeting the V1–V2 region of 16S rRNA genes; 301-bp paired end sequencing of the amplicons was performed on a MiSeq system (Illumina) using a MiSeq Reagent v3 600 cycle kit. The paired end sequences obtained were merged, filtered, and denoised using DADA2. Taxonomic assignment was performed using QIIME2 feature-classifier plugin with the Greengenes 13_8 database. The QIIME2 pipeline, version 2020.2, was used as the bioinformatics environment for the processing of all relevant raw sequencing data. Metagenomic datasets are available at the DNA Data Bank of Japan Sequence Read Archive (DRA010478).

Nontargeted lipidomics

Whole lipids of cultured *H. pylori* SS1 were prepared by single-phase extraction as described by Tsugawa et al. (2020). Briefly, 1.0 × 10^9 CFUs of dried bacterial cells were suspended in 100 µl chloroform. After 1 h incubation, 195 µl methanol and 5 µl EquiSPLASH (Avanti Polar Lipids) were mixed and incubated for another 2 h at room temperature. Thereafter, 20 µl of water was added, and the samples were incubated for 10 min. After extraction, samples were centrifuged at 2,000 ×*g* for 10 min, and the supernatants were collected. The extracted lipids were measured using the ACQUITY UPLC I class system (Waters) coupled with a TripleTOF 6600 (AB Sciex; Tsugawa et al., 2020). Liquid chromatography separation was performed using a reverse-phase column (ACQUITY UPLC BEH C18 column [2.1 mm i.d. × 50 mm, particle size 1.7 µm; Waters]), and data acquisition was performed by data-dependent MS/MS in the negative and positive ion modes. The detected lipid species were annotated using MS-DIAL (Tsugawa et al., 2015) and Peak View (AB Sciex).

Histological analysis

For the assessment of gastric histopathology, two H&E-stained sections per mouse were analyzed for lymphocytic inflammation using a previously described method (Eaton et al., 2007). Briefly, lymphocytic inflammation was defined as inflammatory cell infiltration that displaced the gastric glands. Positive field numbers were divided by the total number of fields and multiplied by 100% to calculate the percentage of the affected fields.

Statistical analysis

An unpaired two-tailed Student's *t* test was used for all the statistical analyses. Asterisks denote level of statistical significance (*, $P < 0.05$; **, $P < 0.01$).

Data availability

The transcriptome RNA-sequencing and metagenomic datasets generated during this study are available at the National Center for Biotechnology Information Gene Expression Omnibus database (GSE136203) and the DNA Data Bank of Japan Sequence Read Archive (DRA010478), respectively.

Online supplemental material

Fig. S1 shows structural analysis of immunostimulatory components in *H. pylori*. Fig. S2 shows cellular and humoral immune responses during *H. pylori* infection. Fig. S3 shows nontargeted lipidomics of helical and coccoid form of *H. pylori*. Fig. S4 shows structural analysis of Spot C. Fig. S5 shows MS spectra of uncharacterized cholesteryl lipid species in *H. pylori*.

Acknowledgments

We thank S. Iwai, S. Torigoe, Y. Hosono, and J. Maaskant for technical support; H. Mimuro, E. Kuroda, T. Watanabe, and M. Ito for discussion; M. Tanaka, Y. Baba, K. Kaseda, and M. Ikawa for embryonic engineering; D. Motooka and D. Okuzaki for bioinformatics analysis; and the Cooperative Research Project Program of the Medical Institute of Bioregulation, Kyushu University, and Genome Information Research Center, Research Institute for Microbial Diseases, Osaka University, for technical support.

This research was supported by the Japan Agency for Medical Research and Development (JP19gm0910010, JP19ak0101070, and JP19fk0108075), Japan Society for the Promotion of Science KAKENHI (JP17H04087 and JP15H05897), the Australian Research Council (DP160100597), and the Takeda Science Foundation.

Author contributions: M. Nagata, E. Ishikawa, B.J. Appelmelk, and S. Yamasaki conceptualized research; M. Nagata, K. Toyonaga, E. Ishikawa, S. Haji, N. Okahashi, M. Takahashi, and T. Miyamoto performed investigations; A. Imamura, K. Takato, H. Ishida, S. Nagai, P. Illarionov, B.L. Stocker, M.S.M. Timmer, D.G.M. Smith, S.J. Williams, and B.J. Appelmelk provided resources; N. Okahashi, M. Takahashi, Y. Izumi, T. Bamba, T. Miyamoto, and M. Arita performed data curation; S. Yamasaki supervised the research; M. Nagata, K. Toyonaga, E. Ishikawa, and S. Yamasaki wrote the manuscript.

Disclosures: The authors declare no competing interests exist.

Submitted: 27 April 2020
Revised: 17 July 2020
Accepted: 18 August 2020

References

Adachi, O., T. Kawai, K. Takeda, M. Matsumoto, H. Tsutsui, M. Sakagami, K. Nakanishi, and S. Akira. 1998. Targeted disruption of the *MyD88* gene results in loss of IL-1- and IL-18-mediated function. *Immunity*. 9: 143–150. https://doi.org/10.1016/S1074-7613(00)80596-8

Adamsson, J., L.S. Ottsjö, S.B. Lundin, A.M. Svennerholm, and S. Raghavan. 2017. Gastric expression of IL-17A and IFNγ in *Helicobacter pylori* infected individuals is related to symptoms. *Cytokine*. 99:30–34. https://doi.org/10.1016/j.cyto.2017.06.013

Antico, A., R. Tozzoli, D. Giavarina, E. Tonutti, and N. Bizzaro. 2012. Hypovitaminosis D as predisposing factor for atrophic type A gastritis: a case-control study and review of the literature on the interaction of Vitamin D with the immune system. *Clin. Rev. Allergy Immunol*. 42:355–364. https://doi.org/10.1007/s12016-011-8255-1

Barnden, M.J., J. Allison, W.R. Heath, and F.R. Carbone. 1998. Defective TCR expression in transgenic mice constructed using cDNA-based α- and β-chain genes under the control of heterologous regulatory elements. *Immunol. Cell Biol.* 76:34–40. https://doi.org/10.1046/j.1440-1711.1998.00709.x

Bimczok, D., R.H. Clements, K.B. Waites, L. Novak, D.E. Eckhoff, P.J. Mannon, P.D. Smith, and L.E. Smythies. 2010. Human primary gastric dendritic cells induce a Th1 response to *H. pylori*. *Mucosal Immunol.* 3:260–269. https://doi.org/10.1038/mi.2010.10

Chang, Y.J., H.Y. Kim, L.A. Albacker, H.H. Lee, N. Baumgarth, S. Akira, P.B. Savage, S. Endo, T. Yamamura, J. Maaskant, et al. 2011. Influenza infection in suckling mice expands an NKT cell subset that protects against airway hyperreactivity. *J. Clin. Invest.* 121:57–69. https://doi.org/10.1172/JCI44845

Cohen, N.R., R.V. Tatituri, A. Rivera, G.F. Watts, E.Y. Kim, A. Chiba, B.B. Fuchs, E. Mylonakis, G.S. Besra, S.M. Levitz, et al. 2011. Innate recognition of cell wall β-glucans drives invariant natural killer T cell responses against fungi. *Cell Host Microbe.* 10:437–450. https://doi.org/10.1016/j.chom.2011.09.011

Cui, J., T. Shin, T. Kawano, H. Sato, E. Kondo, I. Toura, Y. Kaneko, H. Koseki, M. Kanno, and M. Taniguchi. 1997. Requirement for Valpha14 NKT cells in IL-12-mediated rejection of tumors. *Science.* 278:1623–1626. https://doi.org/10.1126/science.278.5343.1623

D'Elios, M.M., A. Amedei, M. Benagiano, A. Azzurri, and G. Del Prete. 2005. *Helicobacter pylori*, T cells and cytokines: the "dangerous liaisons". *FEMS Immunol. Med. Microbiol.* 44:113–119. https://doi.org/10.1016/j.femsim.2004.10.013

Eaton, K.A., M. Mefford, and T. Thevenot. 2001. The role of T cell subsets and cytokines in the pathogenesis of *Helicobacter pylori* gastritis in mice. *J. Immunol.* 166:7456–7461. https://doi.org/10.4049/jimmunol.166.12.7456

Eaton, K.A., S.J. Danon, S. Krakowka, and S.E. Weisbrode. 2007. A reproducible scoring system for quantification of histologic lesions of inflammatory disease in mouse gastric epithelium. *Comp. Med.* 57:57–65.

Ericksen, R.E., S. Rose, C.B. Westphalen, W. Shibata, S. Muthupalani, Y. Tailor, R.A. Friedman, W. Han, J.G. Fox, A.W. Ferrante, Jr., et al. 2014. Obesity accelerates *Helicobacter felis*-induced gastric carcinogenesis by enhancing immature myeloid cell trafficking and TH17 response. *Gut.* 63:385–394. https://doi.org/10.1136/gutjnl-2013-305092

Flornes, L.M., Y.T. Bryceson, A. Spurkland, J.C. Lorentzen, E. Dissen, and S. Fossum. 2004. Identification of lectin-like receptors expressed by antigen presenting cells and neutrophils and their mapping to a novel gene complex. *Immunogenetics.* 56:506–517. https://doi.org/10.1007/s00251-004-0714-x

Frydman, G.H., N. Davis, P.L. Beck, and J.G. Fox. 2015. *Helicobacter pylori* Eradication in Patients with Immune Thrombocytopenic Purpura: A Review and the Role of Biogeography. *Helicobacter.* 20:239–251. https://doi.org/10.1111/hel.12200

Geijtenbeek, T.B., and S.I. Gringhuis. 2016. C-type lectin receptors in the control of T helper cell differentiation. *Nat. Rev. Immunol.* 16:433–448. https://doi.org/10.1038/nri.2016.55

Gray, B.M., C.A. Fontaine, S.A. Poe, and K.A. Eaton. 2013. Complex T cell interactions contribute to *Helicobacter pylori* gastritis in mice. *Infect. Immun.* 81:740–752. https://doi.org/10.1128/IAI.01269-12

Grille, S., A. Zaslawski, S. Thiele, J. Plat, and D. Warnecke. 2010. The functions of steryl glycosides come to those who wait: Recent advances in plants, fungi, bacteria and animals. *Prog. Lipid Res.* 49:262–288. https://doi.org/10.1016/j.plipres.2010.02.001

Haque, M., Y. Hirai, K. Yokota, N. Mori, I. Jahan, H. Ito, H. Hotta, I. Yano, Y. Kanemasa, and K. Oguma. 1996. Lipid profile of *Helicobacter* spp.: presence of cholesteryl glucoside as a characteristic feature. *J. Bacteriol.* 178:2065–2070. https://doi.org/10.1128/JB.178.7.2065-2070.1996

Hara, H., C. Ishihara, A. Takeuchi, T. Imanishi, L. Xue, S.W. Morris, M. Inui, T. Takai, A. Shibuya, S. Saijo, et al. 2007. The adaptor protein CARD9 is essential for the activation of myeloid cells through ITAM-associated and Toll-like receptors. *Nat. Immunol.* 8:619–629. https://doi.org/10.1038/ni1466

Hatakeyama, M. 2004. Oncogenic mechanisms of the *Helicobacter pylori* CagA protein. *Nat. Rev. Cancer.* 4:688–694. https://doi.org/10.1038/nrc1433

Hirai, Y., M. Haque, T. Yoshida, K. Yokota, T. Yasuda, and K. Oguma. 1995. Unique cholesteryl glucosides in *Helicobacter pylori*: composition and structural analysis. *J. Bacteriol.* 177:5327–5333. https://doi.org/10.1128/JB.177.18.5327-5333.1995

Hosoda, K., H. Shimomura, K. Wanibuchi, H. Masui, A. Amgalanbaatar, S. Hayashi, T. Takahashi, and Y. Hirai. 2015. Identification and characterization of a vitamin D_3 decomposition product bactericidal against *Helicobacter pylori*. *Sci. Rep.* 5:8860. https://doi.org/10.1038/srep08860

Ito, Y., J.L. Vela, F. Matsumura, H. Hoshino, A. Tyznik, H. Lee, E. Girardi, D.M. Zajonc, R. Liddington, M. Kobayashi, et al. 2013. *Helicobacter pylori* cholesteryl α-glucosides contribute to its pathogenicity and immune response by natural killer T cells. *PLoS One.* 8. e78191. https://doi.org/10.1371/journal.pone.0078191

Jan, H.M., Y.C. Chen, Y.Y. Shih, Y.C. Huang, Z. Tu, A.B. Ingle, S.W. Liu, M.S. Wu, J. Gervay-Hague, K.T. Mong, et al. 2016. Metabolic labelling of cholesteryl glucosides in *Helicobacter pylori* reveals how the uptake of human lipids enhances bacterial virulence. *Chem. Sci. (Camb.).* 7:6208–6216. https://doi.org/10.1039/C6SC00889E

Kabuye, D., Y. Chu, W. Lao, G. Jin, and H. Kang. 2019. Association between *CLEC4E* gene polymorphism of mincle and pulmonary tuberculosis infection in a northern Chinese population. *Gene.* 710:24–29. https://doi.org/10.1016/j.gene.2019.05.011

Kawakubo, M., Y. Ito, Y. Okimura, M. Kobayashi, K. Sakura, S. Kasama, M.N. Fukuda, M. Fukuda, T. Katsuyama, and J. Nakayama. 2004. Natural antibiotic function of a human gastric mucin against *Helicobacter pylori* infection. *Science.* 305:1003–1006. https://doi.org/10.1126/science.1099250

Kawamura, A., E. Takeda, N. Tanida, K. Nakagawa, H. Yamamoto, K. Sawada, and T. Okano. 2006. Inhibitory Effect of Long Term 1α-Hydroxyvitamin D_3 Administration on *Helicobacter pylori* Infection. *J. Clin. Biochem. Nutr.* 38:103–106. https://doi.org/10.3164/jcbn.38.103

Kiyotake, R., M. Oh-Hora, E. Ishikawa, T. Miyamoto, T. Ishibashi, and S. Yamasaki. 2015. Human Mincle Binds to Cholesterol Crystals and Triggers Innate Immune Responses. *J. Biol. Chem.* 290:25322–25332. https://doi.org/10.1074/jbc.M115.645234

Labenz, J. 2001. Current role of acid suppressants in *Helicobacter pylori* eradication therapy. *Best Pract. Res. Clin. Gastroenterol.* 15:413–431. https://doi.org/10.1053/bega.2001.0188

Lantz, O., and A. Bendelac. 1994. An invariant T cell receptor α chain is used by a unique subset of major histocompatibility complex class I-specific $CD4^+$ and $CD4^-8^-$ T cells in mice and humans. *J. Exp. Med.* 180:1097–1106. https://doi.org/10.1084/jem.180.3.1097

Lebrun, A.H., C. Wunder, J. Hildebrand, Y. Churin, U. Zähringer, B. Lindner, T.F. Meyer, E. Heinz, and D. Warnecke. 2006. Cloning of a cholesterol-α-glucosyltransferase from *Helicobacter pylori*. *J. Biol. Chem.* 281:27765–27772. https://doi.org/10.1074/jbc.M603345200

Lobato-Pascual, A., P.C. Saether, S. Fossum, E. Dissen, and M.R. Daws. 2013. Mincle, the receptor for mycobacterial cord factor, forms a functional receptor complex with MCL and FcεRI-γ. *Eur. J. Immunol.* 43:3167–3174. https://doi.org/10.1002/eji.201343752

Lu, X., M. Nagata, and S. Yamasaki. 2018. Mincle: 20 years of a versatile sensor of insults. *Int. Immunol.* 30:233–239. https://doi.org/10.1093/intimm/dxy028

Matsui, H., T. Takahashi, S.Y. Murayama, I. Uchiyama, K. Yamaguchi, S. Shigenobu, T. Matsumoto, M. Kawakubo, K. Horiuchi, H. Ota, et al. 2014. Development of new PCR primers by comparative genomics for the detection of *Helicobacter suis* in gastric biopsy specimens. *Helicobacter.* 19:260–271. https://doi.org/10.1111/hel.12127

Mayberry, W.R., and P.F. Smith. 1983. Structures and properties of acyl diglucosylcholesterol and galactofuranosyl diacylglycerol from *Acholeplasma axanthum*. *Biochim. Biophys. Acta.* 752:434–443. https://doi.org/10.1016/0005-2760(83)90273-4

McGee, D.J., A.E. George, E.A. Trainor, K.E. Horton, E. Hildebrandt, and T.L. Testerman. 2011. Cholesterol enhances *Helicobacter pylori* resistance to antibiotics and LL-37. *Antimicrob. Agents Chemother.* 55:2897–2904. https://doi.org/10.1128/AAC.00016-11

Miyake, Y., K. Toyonaga, D. Mori, S. Kakuta, Y. Hoshino, A. Oyamada, H. Yamada, K. Ono, M. Suyama, Y. Iwakura, et al. 2013. C-type lectin MCL is an FcRγ-coupled receptor that mediates the adjuvanticity of mycobacterial cord factor. *Immunity.* 38:1050–1062. https://doi.org/10.1016/j.immuni.2013.03.010

Miyake, Y., O.H. Masatsugu, and S. Yamasaki. 2015. C-Type Lectin Receptor MCL Facilitates Mincle Expression and Signaling through Complex Formation. *J. Immunol.* 194:5366–5374. https://doi.org/10.4049/jimmunol.1402429

Morey, P., L. Pfannkuch, E. Pang, F. Boccellato, M. Sigal, A. Imai-Matsushima, V. Dyer, M. Koch, H.J. Mollenkopf, P. Schlaermann, et al. 2018. *Helicobacter pylori* Depletes Cholesterol in Gastric Glands to Prevent Interferon Gamma Signaling and Escape the Inflammatory Response. *Gastroenterology.* 154:1391–1404.e9. https://doi.org/10.1053/j.gastro.2017.12.008

Nagai, S., H. Mimuro, T. Yamada, Y. Baba, K. Moro, T. Nochi, H. Kiyono, T. Suzuki, C. Sasakawa, and S. Koyasu. 2007. Role of Peyer's patches in the induction of *Helicobacter pylori*-induced gastritis. *Proc. Natl. Acad. Sci. USA*. 104:8971–8976. https://doi.org/10.1073/pnas.0609014104

Nagata, M., Y. Izumi, E. Ishikawa, R. Kiyotake, R. Doi, S. Iwai, Z. Omahdi, T. Yamaji, T. Miyamoto, T. Bamba, et al. 2017. Intracellular metabolite β-glucosylceramide is an endogenous Mincle ligand possessing immunostimulatory activity. *Proc. Natl. Acad. Sci. USA*. 114:E3285–E3294. https://doi.org/10.1073/pnas.1618133114

NIH Consensus Conference. 1994. *Helicobacter pylori* in peptic ulcer disease. NIH Consensus Development Panel on *Helicobacter pylori* in Peptic Ulcer Disease. *JAMA*. 272:65–69. https://doi.org/10.1001/jama.272.1.65

Noach, L.A., T.M. Rolf, and G.N. Tytgat. 1994. Electron microscopic study of association between *Helicobacter pylori* and gastric and duodenal mucosa. *J. Clin. Pathol*. 47:699–704. https://doi.org/10.1136/jcp.47.8.699

Omahdi, Z., Y. Horikawa, M. Nagae, K. Toyonaga, A. Imamura, K. Takato, T. Teramoto, H. Ishida, Y. Kakuta, and S. Yamasaki. 2020. Structural insight into the recognition of pathogen-derived phosphoglycolipids by C-type lectin receptor DCAR. *J. Biol. Chem*. 295:5807–5817. https://doi.org/10.1074/jbc.RA120.012491

Park, S.Y., S. Ueda, H. Ohno, Y. Hamano, M. Tanaka, T. Shiratori, T. Yamazaki, H. Arase, N. Arase, A. Karasawa, et al. 1998. Resistance of Fc receptor- deficient mice to fatal glomerulonephritis. *J. Clin. Invest*. 102:1229–1238. https://doi.org/10.1172/JCI3256

Peek, R.M., Jr., and M.J. Blaser. 2002. *Helicobacter pylori* and gastrointestinal tract adenocarcinomas. *Nat. Rev. Cancer*. 2:28–37. https://doi.org/10.1038/nrc703

Poursina, F., J. Faghri, S. Moghim, H. Zarkesh-Esfahani, B. Nasr-Esfahani, H. Fazeli, A. Hasanzadeh, and H.G. Safaei. 2013. Assessment of cagE and babA mRNA expression during morphological conversion of *Helicobacter pylori* from spiral to coccoid. *Curr. Microbiol*. 66:406–413. https://doi.org/10.1007/s00284-012-0280-7

Roy, C.R., and E.S. Mocarski. 2007. Pathogen subversion of cell-intrinsic innate immunity. *Nat. Immunol*. 8:1179–1187. https://doi.org/10.1038/ni1528

Shimamura, M. 2012. Immunological functions of steryl glycosides. *Arch. Immunol. Ther. Exp. (Warsz.)*. 60:351–359. https://doi.org/10.1007/s00005-012-0190-1

Shimomura, H., K. Hosoda, and Y. Hirai. 2013. Interaction of *Helicobacter pylori* Cell Membrane with Non-Esterified Cholesterol and Other Steroids. *Open J. Med. Microbiol*. 3:70–79. https://doi.org/10.4236/ojmm.2013.31011

Tannaes, T., H.J. Grav, and G. Bukholm. 2000. Lipid profiles of *Helicobacter pylori* colony variants. *APMIS*. 108:349–356. https://doi.org/10.1034/j.1600-0463.2000.d01-67.x

Toyonaga, K., S. Torigoe, Y. Motomura, T. Kamichi, J.M. Hayashi, Y.S. Morita, N. Noguchi, Y. Chuma, H. Kiyohara, K. Matsuo, et al. 2016. C-Type Lectin Receptor DCAR Recognizes Mycobacterial Phosphatidyl-Inositol Mannosides to Promote a Th1 Response during Infection. *Immunity*. 45:1245–1257. https://doi.org/10.1016/j.immuni.2016.10.012

Tsugawa, H., K. Ikeda, M. Takahashi, A. Satoh, Y. Mori, H. Uchino, N. Okahashi, Y. Yamada, I. Tada, P. Bonini, et al. 2020. A lipidome atlas in MS-DIAL 4. *Nat. Biotechnol*. https://doi.org/10.1038/s41587-020-0531-2

Tsugawa, H., T. Cajka, T. Kind, Y. Ma, B. Higgins, K. Ikeda, M. Kanazawa, J. VanderGheynst, O. Fiehn, and M. Arita. 2015. MS-DIAL: data-independent MS/MS deconvolution for comprehensive metabolome analysis. *Nat. Methods*. 12:523–526. https://doi.org/10.1038/nmeth.3393

Wu, W., Y. Yang, and G. Sun. 2012. Recent Insights into Antibiotic Resistance in *Helicobacter pylori* Eradication. *Gastroenterol. Res. Pract*. 2012. 723183. https://doi.org/10.1155/2012/723183

Wunder, C., Y. Churin, F. Winau, D. Warnecke, M. Vieth, B. Lindner, U. Zähringer, H.J. Mollenkopf, E. Heinz, and T.F. Meyer. 2006. Cholesterol glucosylation promotes immune evasion by *Helicobacter pylori*. *Nat. Med*. 12:1030–1038. https://doi.org/10.1038/nm1480

Yamasaki, S., E. Ishikawa, M. Sakuma, H. Hara, K. Ogata, and T. Saito. 2008. Mincle is an ITAM-coupled activating receptor that senses damaged cells. *Nat. Immunol*. 9:1179–1188. https://doi.org/10.1038/ni.1651

Yamasaki, S., M. Matsumoto, O. Takeuchi, T. Matsuzawa, E. Ishikawa, M. Sakuma, H. Tateno, J. Uno, J. Hirabayashi, Y. Mikami, et al. 2009. C-type lectin Mincle is an activating receptor for pathogenic fungus, *Malassezia*. *Proc. Natl. Acad. Sci. USA*. 106:1897–1902. https://doi.org/10.1073/pnas.0805177106

Yonekawa, A., S. Saijo, Y. Hoshino, Y. Miyake, E. Ishikawa, M. Suzukawa, H. Inoue, M. Tanaka, M. Yoneyama, M. Oh-Hora, et al. 2014. Dectin-2 is a direct receptor for mannose-capped lipoarabinomannan of mycobacteria. *Immunity*. 41:402–413. https://doi.org/10.1016/j.immuni.2014.08.005

Zhao, X.Q., L.L. Zhu, Q. Chang, C. Jiang, Y. You, T. Luo, X.M. Jia, and X. Lin. 2014. C-type lectin receptor dectin-3 mediates trehalose 6,6′-dimycolate (TDM)-induced Mincle expression through CARD9/Bcl10/MALT1-dependent nuclear factor (NF)-κB activation. *J. Biol. Chem*. 289:30052–30062. https://doi.org/10.1074/jbc.M114.588574

Supplemental material

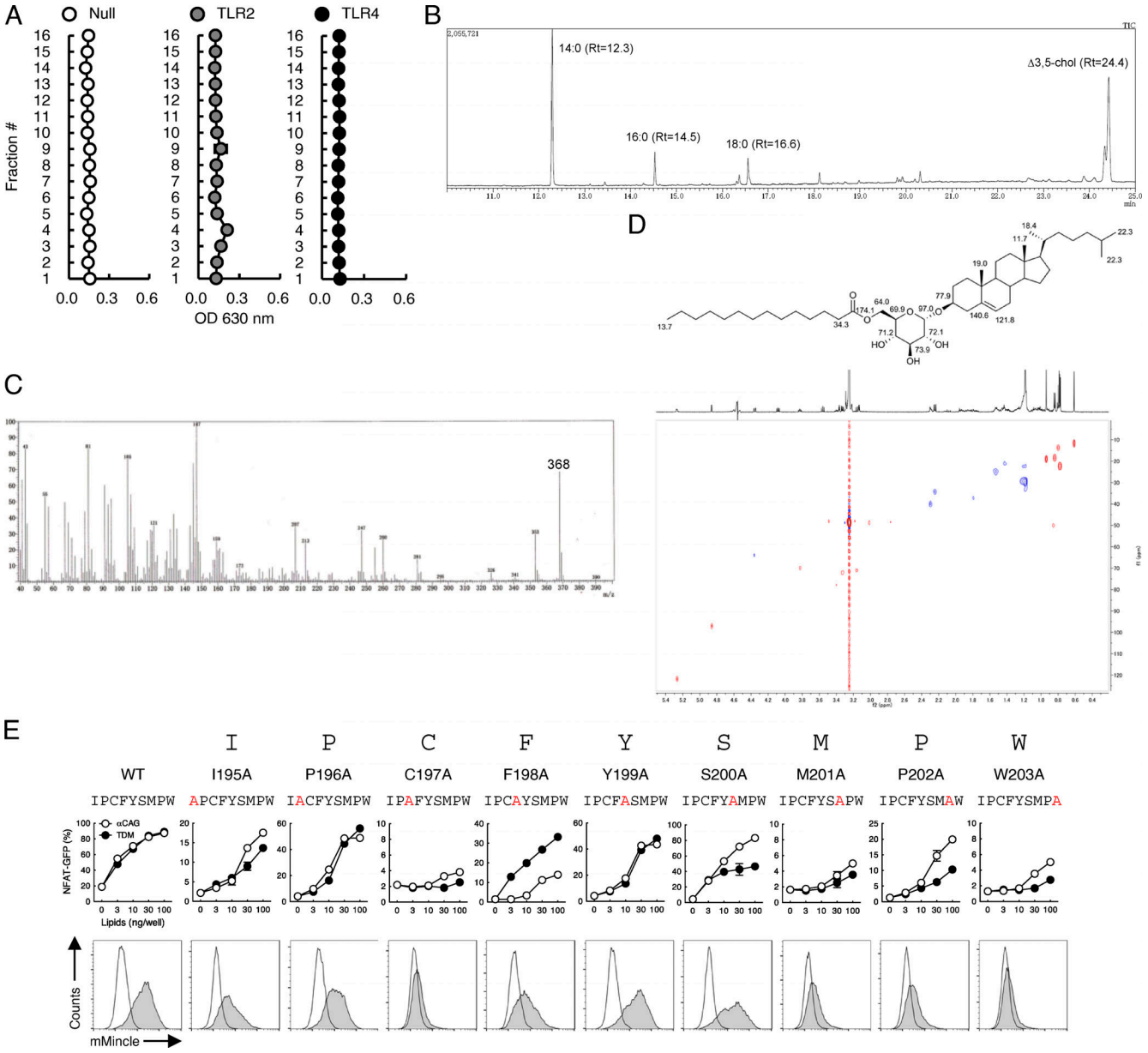

Figure S1. **Identification of chemical structure of fraction 13-14 as αCAG. (A)** HEK-based NF-κB reporter cells expressing TLR2 or TLR4 were stimulated with HPTLC-separated lipid fractions from *H. pylori* for 20 h. Activation of NF-κB was assessed by monitoring SEAP activity in the supernatants. **(B)** GC-MS chromatogram of FAMEs and sterol derived from fraction 13-14. **(C)** MS spectrum of 24.4 min in B. **(D)** ^{13}C-NMR chemical shifts of fraction 13-14 (upper panel) were assigned by HSQC (lower panel) and HMBC experiments. **(E)** NFAT-GFP reporter cells expressing FcRγ + Flag-tagged Mincle mutants generated by site-directed mutagenesis were stimulated with indicated lipids for 20 h. Induction of GFP was analyzed by flow cytometry (upper panels). Cell surface expression of Mincle was detected by anti-Flag mAb (lower panels). Open histograms show staining with isotype control. The spectrum of binding preferences for the mutants was distinct; in particular, the F198A mutation did not affect TDM recognition, while this mutant poorly recognized αCAG. In contrast, S200A and P202A selectively impaired TDM binding. Note that the C197 is considered to be involved in intramolecular disulfide bonds. Data are presented as the mean ± SD of duplicate assays (A and E).

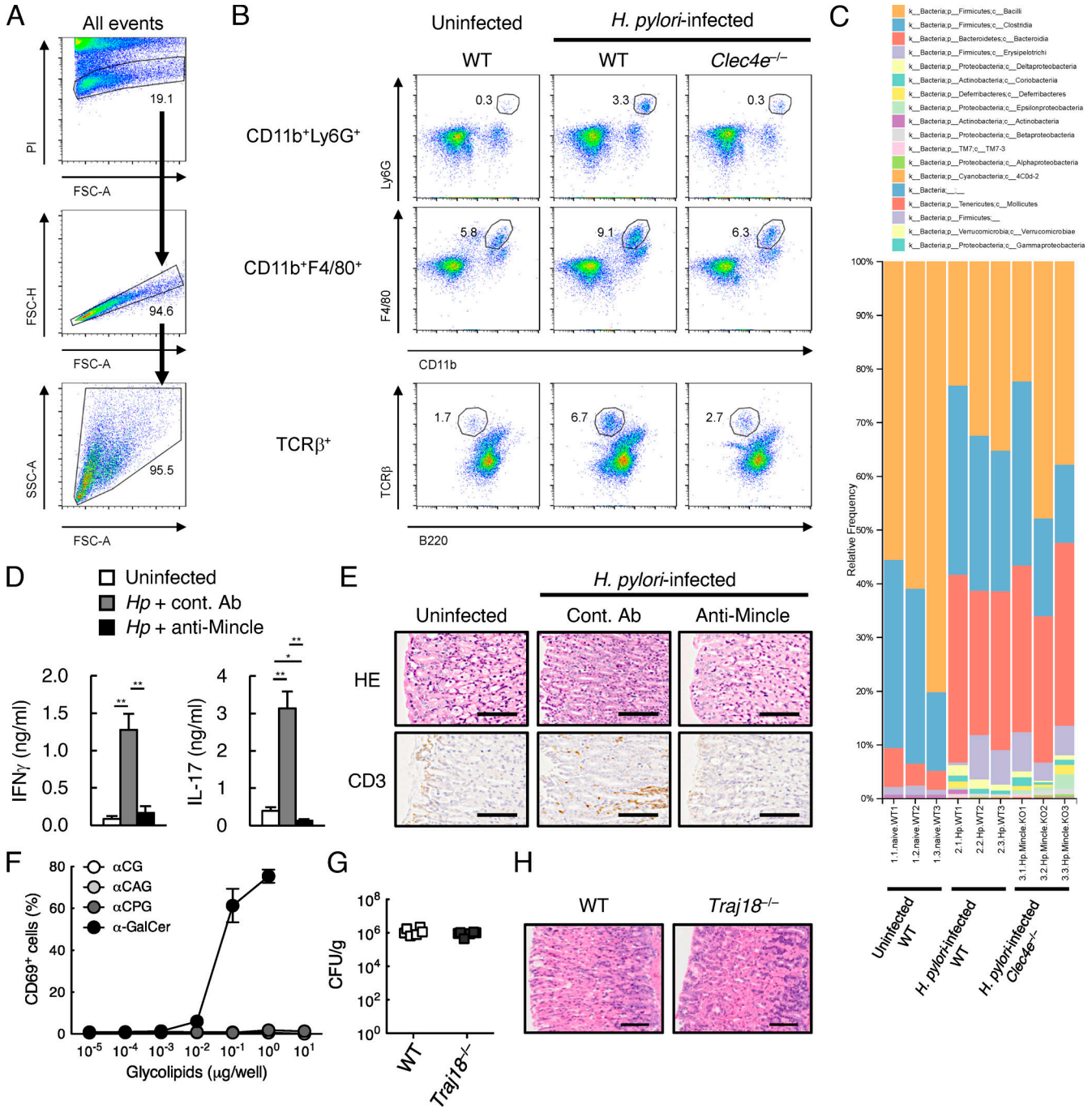

Figure S2. **Cellular immunity during *H. pylori* infection. (A)** Gating strategy for analyzing gastric MNCs by flow cytometry. Numbers indicate the percentages of cells in each gate. PI, propidium iodide; SSC, side scatter; FSC, forward scatter. **(B)** Gastric MNCs from uninfected and *H. pylori*–infected WT or *Clec4e*$^{-/-}$ mice were stained with anti-Ly6G, F4/80, CD11b, TCRβ and B220 at 6 wk after infection. Numbers indicate the percentages of cells in each gate. **(C)** Metagenome analysis of gastric mucosal swabs from uninfected WT mice, *H. pylori*–infected WT and *Clec4e*$^{-/-}$ mice (n = 3 in each group) after 12 wk. **(D)** *H. pylori*–infected WT mice were injected with anti-Mincle mAb or rat IgG as a control Ab (cont. Ab). At 8 wk after infection, Peyer's patch cells were collected and cultured for 4 d in the absence of exogenous *H. pylori* lysates. Uninfected WT mice were used as control. The concentrations of IFN-γ and IL-17 in the supernatants were determined by ELISA. **(E)** H&E (HE) staining and immunohistochemical staining with anti-CD3 of stomach sections from uninfected and *H. pylori*–infected mice treated with anti-Mincle mAb or control Ab. Scale bar, 100 µm. **(F)** Mouse invariant NKT hybridoma cells (DN32.D3) expressing CD1d were incubated with indicated amounts of αCG, αCAG, αCPG, or α-GalCer for 1 d. Each lipid was dissolved in DMSO. The expressions of CD69 were analyzed by flow cytometry. **(G)** The number of bacteria recovered from the stomachs of WT and *Traj18*$^{-/-}$ mice at 8 wk after *H. pylori* infection. Bacterial numbers were determined by counting the number of colonies on *H. pylori* selective agar plates. **(H)** H&E staining of stomach sections from *H. pylori*–infected WT and *Traj18*$^{-/-}$ mice after 8 wk. Scale bar, 100 µm. Data are presented as the mean ± SD of triplicate assays (D and F) from two independent experiments (at least six infected mice in each group) with similar results. An unpaired two-tailed Student's *t* test was used for the statistical analyses. *, P < 0.05; **, P < 0.01.

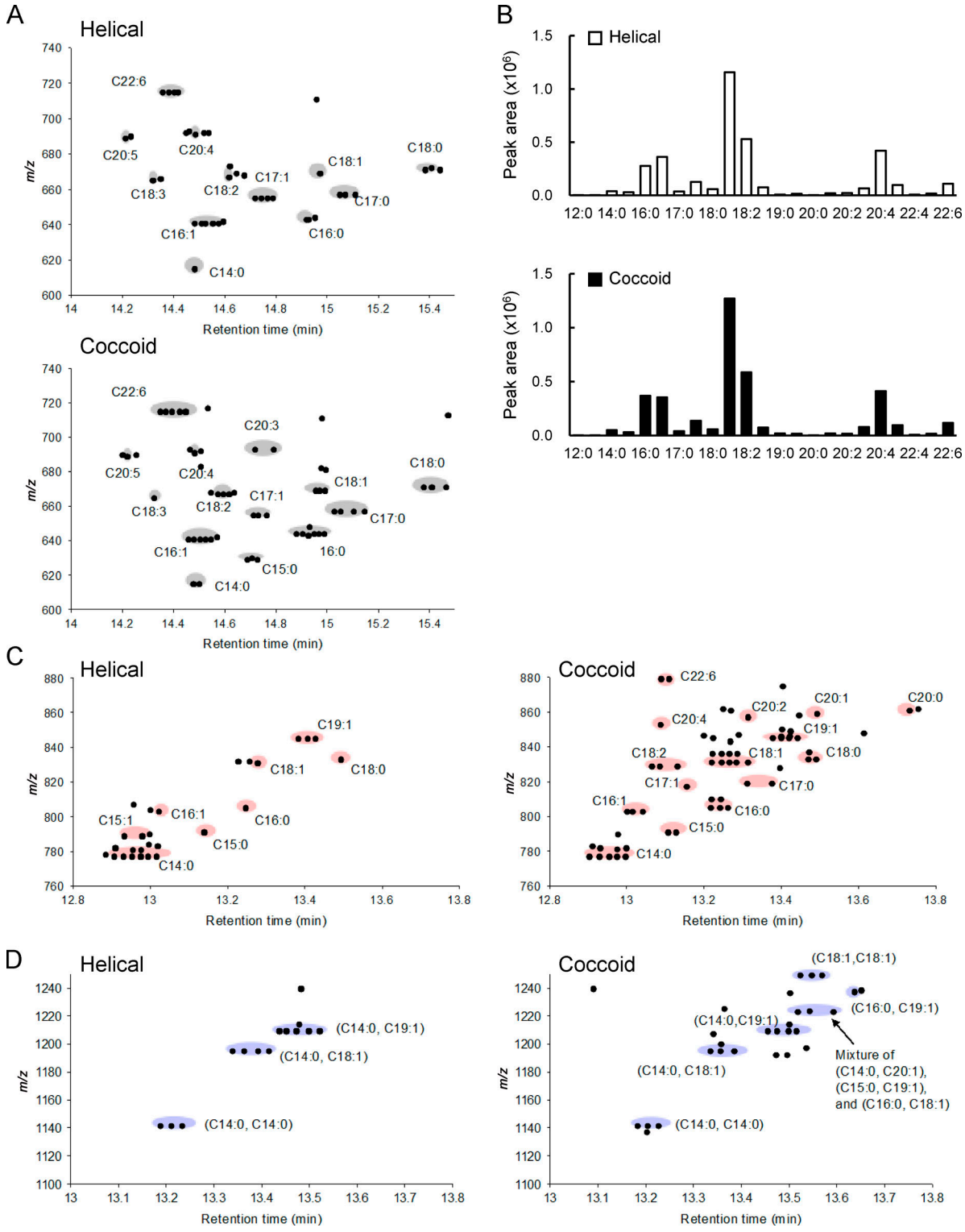

Figure S3. **Lipidomics of helical and coccoid form of *H. pylori*. (A)** 2D map of mass (*m/z* of precursor ions) versus LC retention time of fatty acids focused on the cholesterol ester isolated from the helical (upper panel) or coccoid (lower panel) form of *H. pylori*. The 2D map consists of the *m/z* values of the precursor ions along the vertical axis and the retention times along the horizontal axis. **(B)** Peak area of each fatty acid fragment ion analyzed in A. **(C and D)** 2D map of mass (*m/z* of precursor ions) versus liquid chromatography retention time of fatty acids focused on αCAG (C) and αCPG (D) isolated from the helical (left panels) or coccoid (right panels) forms of *H. pylori*. The 2D map consists of the *m/z* values of the precursor ions along the vertical axis and the retention time along the horizontal axis.

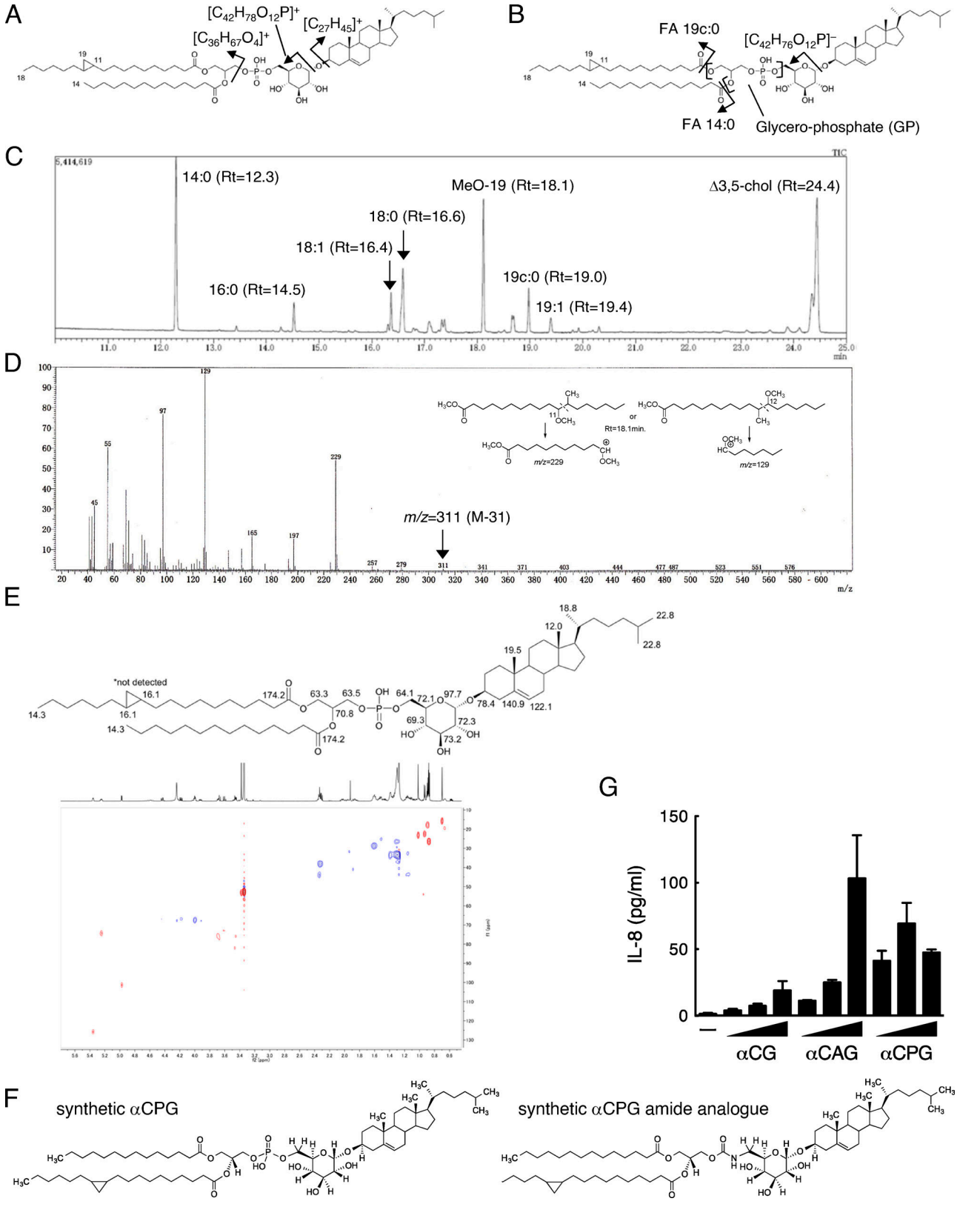

Figure S4. **Determination of the chemical structure of Spot C as αCPG. (A)** Scheme of the cleavage site of Spot C in Fig. 4 K in the positive ion mode of MS/MS analysis. **(B)** Scheme of the cleavage site of Spot C in Fig. 4 L in the negative ion mode of MS/MS analysis. **(C)** GC-MS FAME analysis of Spot C after methanolysis. **(D)** MS spectrum of MeO-19 at 18.1 min in C. **(E)** ^{13}C-NMR chemical shift assignment of Spot C (upper panel). Each chemical shift was assigned by HSQC (lower panel) and HMBC experiments. **(F)** Chemical structure of the synthesized αCPG (C14:0 19c:0; left panel) and synthesized αCPG amide analogue (right panel). **(G)** hMoDCs were stimulated with indicated amounts αCG, αCAG, or αCPG (0.1, 0.3, and 1 nmol/well) for 1 d. The concentrations of IL-8 in the supernatants were determined by ELISA. Data are presented as the mean ± SD of triplicate assays (G).

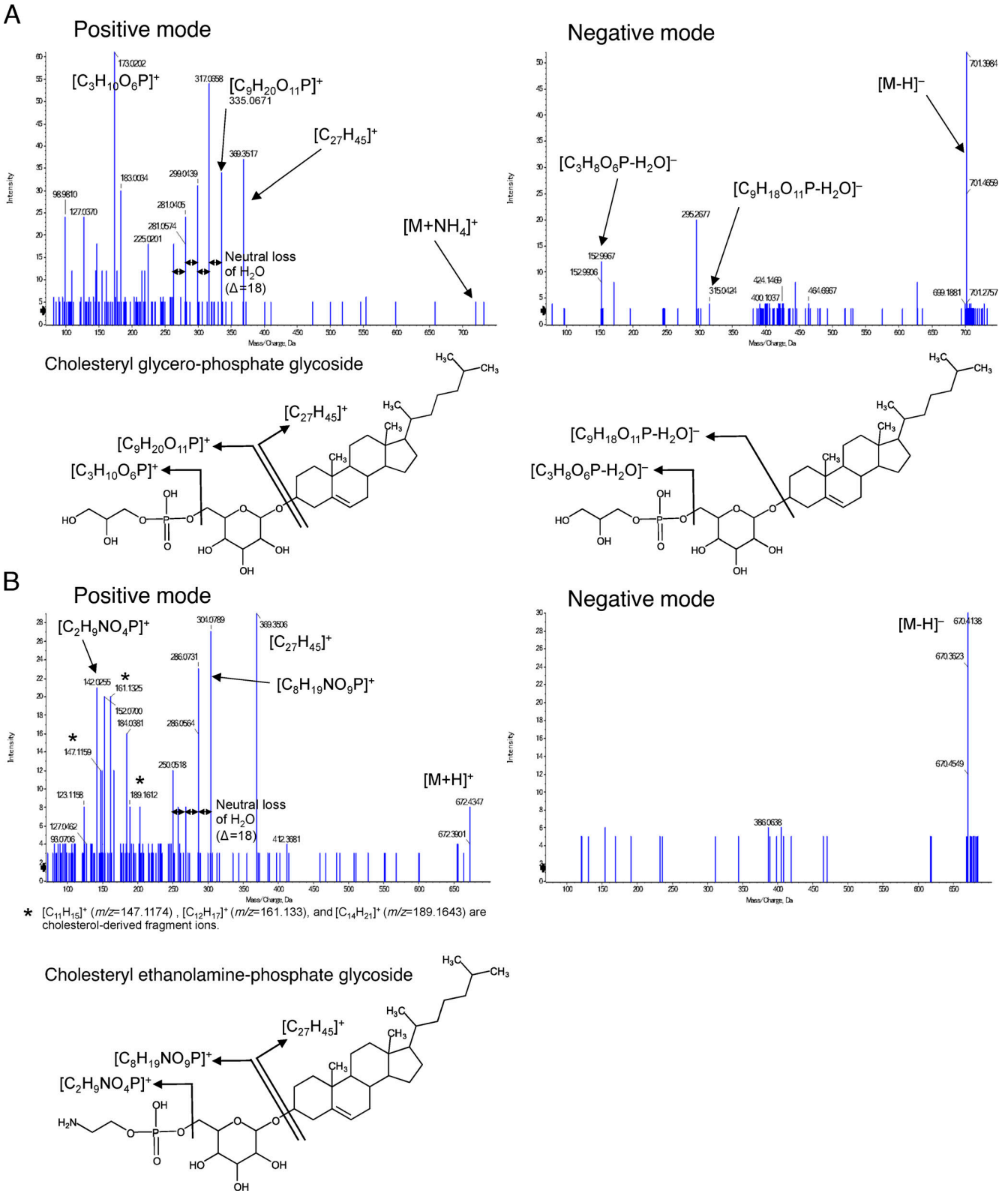

Figure S5. **Identification of uncharacterized cholesteryl lipid species in *H. pylori*. (A and B)** MS spectra of cholesteryl glycero-phosphate glycoside (A, upper panels) and cholesteryl ethanolamine-phosphate glycoside (B, upper panels). Schemes of the cleavage site are shown in the lower panels.